

AD No. 28258
ASTIA FILE COPY

Not used

Office of Naval Research

Contract N50RI-76 • Task Order No.1 • NR-078-011

AN EXPERIMENTAL INVESTIGATION
OF THE TRANSMISSION PROPERTIES OF
THE DOMINANT CIRCULAR-ELECTRIC MODE



By

Leonard S. Sheingold

September 1, 1953

Technical Report No. 167

Cruft Laboratory
Harvard University
Cambridge, Massachusetts

THIS REPORT HAS BEEN DELIMITED
AND CLEARED FOR PUBLIC RELEASE
UNDER DOD DIRECTIVE 5200.20 AND
NO RESTRICTIONS ARE IMPOSED UPON
ITS USE AND DISCLOSURE,

DISTRIBUTION STATEMENT A

APPROVED FOR PUBLIC RELEASE;
DISTRIBUTION UNLIMITED.

ERRATA

for

Cruft Laboratory Technical Report

No. 178

The Collinear Antenna Array: Theory and Measurements

Howard W. Andrews

Table of Contents, II, 5 "singly"-driven
IV, 5 γ -integral

p. 18, line 5: Add] after $-2 \sin \beta (h-g)$

p. 19, line 1: change to $S(\beta a, 2\beta g)$

p. 20, line 6: change to $\overline{C}(\beta a, 2\beta g)$

p. 22, line 2, Sec. 5: Fig. 2-2b should be Fig. 2b.

p. 22, last line: $\dots [2\overline{C}_c(\beta a, \beta h) - \overline{C}_c(\beta a, 2\beta h)]$

p. 27, line 7 from bottom: right-hand side of equation should be

$$\sin^2 h^2 (aw_m + \rho_s \pm a\delta\omega) + \sin^2 \beta \delta w$$

p. 28, line 7 from top:

$$\left(\frac{a}{\beta}\right)^2 \sinh^2 2(aw_m + \rho_s) = \dots$$

p. 39, line 3 from bottom: Second integral should be

$$\int_g^h$$

p. 43, line 5 from bottom should read:

$$\sin \beta g [S_g(\beta a, \beta (c-g)) \dots$$

p. 45, line 1: right-hand side of equation should read:

$$\int_b^c \sin \beta z K(z, g) dz$$

p. 45, last line: right-hand side of equation should read

$$f[C_g(w), \overline{C}_c(x), \overline{C}(y), \sin z] - \dots$$

p. 46, line 1: change to $C_g, \overline{C}_c, \overline{C}$

Office of Naval Research

Contract N5ori-76

Task Order No. 1

NR-078-011

Technical Report

on

An Experimental Investigation of the Transmission
Properties of the Dominant Circular-Electric Mode

by

Leonard S. Sheingold

September 1, 1953

The research reported in this document was made possible through support extended Cruft Laboratory, Harvard University, jointly by the Navy Department (Office of Naval Research), the Signal Corps of the U. S. Army, and the U. S. Air Force, under ONR Contract N5ori-76, T. O. 1 and 28.

Technical Report No. 167

Cruft Laboratory

Harvard University

Cambridge, Massachusetts

An Experimental Investigation of the Transmission
Properties of the Dominant Circular-Electric Mode

by

Leonard S. Sheingold

Graft Laboratory, Harvard University

Cambridge, Massachusetts

Abstract

A novel method of measuring impedance in a circular waveguide supporting only the dominant circular-electric mode is described. A complete description of the experimental arrangement used in the TE_{01} impedance measurements is presented. Results are given of precise impedance measurements made on circular obstacles, circumferential gaps and radiating guides. These experimental results are compared with theoretical values and are found to be in excellent agreement. It is demonstrated that application of Deschamps' graphical method in the experimental determination of the scattering parameters of a circumferential-gap-junction results in a rapid determination of the pertinent quantities; i.e., the power reflected by, power transmitted through, and power dissipated in the junction.

I.

TE_{01} IMPEDANCE MEASUREMENTS

The TE_{01} Transmission Line

A circular waveguide with only the TE_{01} mode propagating can be considered in terms of an equivalent transmission line with appropriate line voltages and currents. It can be shown that the field components of the circular-electric modes can be expressed using appropriate modal voltages and modal currents.¹ If the dominant circular-electric mode is alone present in the circular waveguide, the field components are given by

$$E_{\phi}(r, z) = \frac{J_1(\rho_1 r/a)}{\sqrt{\pi} a J_0(\rho_1)} V_1(z)$$

$$\begin{aligned}
 H_r(r, z) &= - \frac{J_1(\rho_1 r/a)}{\sqrt{\pi} a J_0(\rho_1)} I_1(z) \\
 H_z(r, z) &= - \frac{j \eta_0 \rho_1 J_0(\rho_1 r/a)}{ka^2 \sqrt{\pi} J_0(\rho_1)} V_1(z) \\
 E_r(r, z) &= E_z(r, z) = H_\phi(r, z) = 0
 \end{aligned}$$

Substitution of these field components into Maxwell's Equations results in the conventional transmission-line equations

$$\begin{aligned}
 \frac{dV_1(z)}{dz} &= -j\gamma_1 Z_{cl} I_1(z) \\
 \frac{dI_1(z)}{dz} &= -j\gamma_1 Y_{cl} V_1(z)
 \end{aligned}$$

where the characteristic admittance Y_{cl} and the characteristic impedance Z_{cl} are defined by

$$Y_{cl} = \frac{1}{Z_{cl}} = \frac{\sqrt{k^2 - (\rho_1/a)^2}}{\omega \mu}$$

and

$$\gamma_1 = \sqrt{k^2 - (\rho_1/a)^2}$$

where $\rho_1 = 3.8317$ corresponds to the first zero of the Bessel function of the first order.

Since a transmission-line analogy has been established, a means for measuring impedance in the circular waveguide can be devised.

A slotted-section and a travelling-probe are generally used in waveguide

impedance measurements. The method in which the detector is moved along the transmission line is "the standing-wave method". This method of measurement cannot be employed here since the solely transverse wall currents of the circular-electric mode would excite the slot and the energy inside the circular guide would be partially radiated. In addition, the presence of the slot would create an asymmetry in the geometry of the waveguide structure. This asymmetry would convert energy from the TE_{01} mode to lower order modes which would propagate.

The resonance-curve method in which the length of the line is varied by moving the position of the generator with respect to a fixed detector and a fixed load, is the simplest way to make impedance measurements on the " TE_{01} transmission line".

Referring to the basic transmission line equations, it is observed that the transmission line current $I_1(z)$ is proportional to $H_r(r, z)$ and the transmission line voltage $V_1(z)$ is proportional to $H_z(r, z)$ (or $E_\phi(r, z)$). This implies that if suitable magnetic probes were available, it would be possible to measure the equivalent current or voltage on the waveguide transmission line.

In the following sections a description is given of the circular waveguide, the detecting and generating devices, and other components which make up the " TE_{01} transmission line".

Circular Waveguide

The circular waveguide is standard commercial brass tubing with an inner diameter of 5.755 inches ($\pm .005$ inch) and 0.125 inch wall thickness. The large inner diameter was chosen because of the availability of experimental equipment in the 10 centimeter range. Also, the large diameter tubing insures that the perturbation of the electromagnetic fields by probing devices may be kept small. At a free space wavelength of 10 centimeters the waveguide is capable of supporting six waveguide modes. (TE_{11} , TM_{01} , TE_{21} , TE_{01} , TM_{11} , TE_{31})

The circular waveguide consists of several individual sections of tubing joined together by specially designed flanges. The flanges were designed so that a thin planar obstacle could be inserted at a convenient location in the

waveguide.

Generator Assembly

The generator consists of a shielded loop of 3/16 inch diameter constructed from a 1/32 inch o.d. coaxial line. The generator loop is mounted on the face of a non-contacting short-circuiting piston and is oriented and positioned to couple maximum energy to the desired dominant circular-electric mode. To obtain the maximum coupling, the axis of the shielded loop is oriented in the radial direction and the plane of the loop is perpendicular to the plane of the plunger. The radial position of the exciting loop is determined by calculating the radius at which the radial component of the magnetic field near the surface of the wall of the piston is at its maximum. The optimum radius, r_{mc} , is readily obtained by differentiating $H_r(r,z)$ with respect to r and setting the resulting expression equal to zero. The maximum value of the function between its first and second zero occurs at

$$\frac{p_1 r_{mc}}{a} = 1.841$$

therefore, the radial position of the exciting loop corresponding to the position of maximum coupling to the dominant circular-electric mode is

$$r_{mc} = 0.480 a$$

and for $2a$ equal to 5.755 inches

$$r_{mc} = 1.381 \text{ in.}$$

A photograph of the generator loop which is identical to the shielded loops used in the detecting section is shown in Fig. 1. A drawing of the cross section of the loop is shown in Fig. 2. Since the gap of 0.016 in. is extremely small compared to wavelength (i.e., 0.0022λ at $\lambda = 10$ cm.), the balanced operation of the loop is virtually independent of the distance from the gap to the position of the short circuit.² This balanced shielded loop may be considered as a current probe capable of exciting or

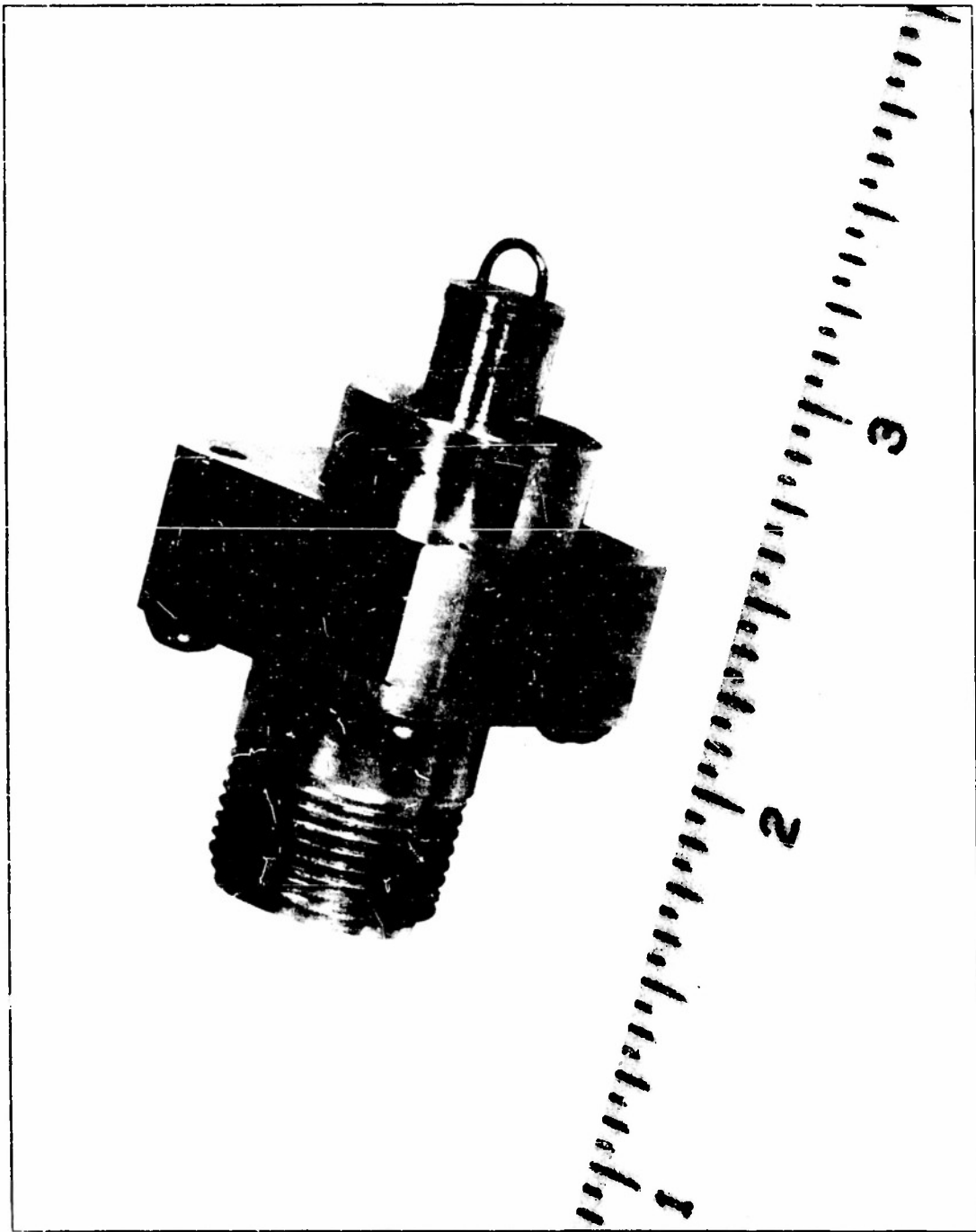


FIG. 1 SHIELDED LOOP USED IN GENERATOR AND DETECTOR ASSEMBLIES

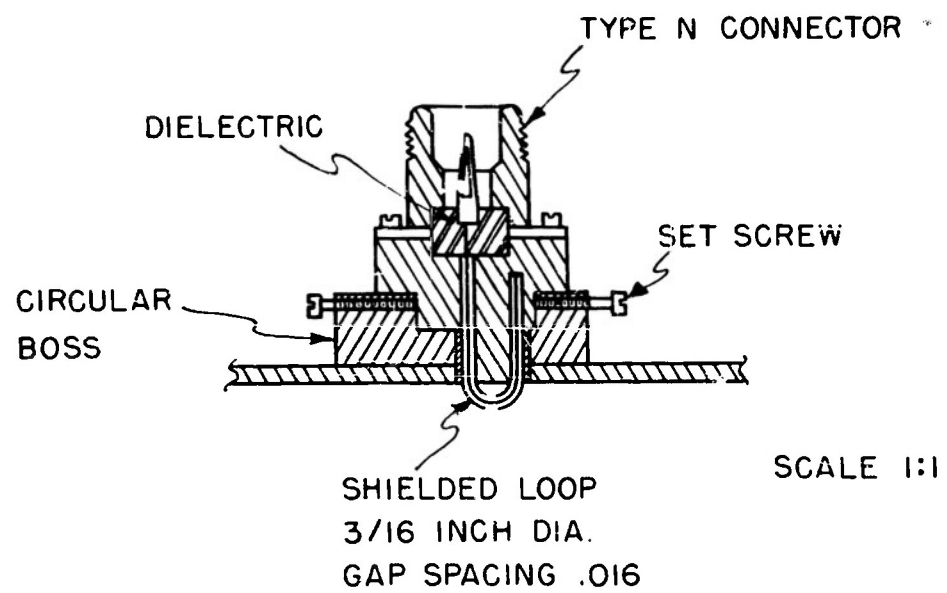


FIG. 2 CROSS-SECTION OF SHIELDED LOOP

detecting currents on the surface of the guide walls. In the transmission-line approach, the generating loop is a current generator (loosely coupled) with its current strength proportional to the area of the loop.

Short-Circuiting Pistons

The current generator is mounted on a brass end plate which is attached to a textolite cylinder as shown in the photograph of Fig. 3 and the drawing of Fig. 4.

The currents associated with the circular-electric modes are purely transverse on the side wall of the waveguide and are in the ϕ direction on the end wall of the short circuiting piston. The surface currents tend to vanish at the junction of the waveguide and the short-circuiting piston. Owing to the vanishing currents at the junction, a short-circuiting plunger can be used which does not make contact with the side wall. Obviously, a non-contacting short-circuiting plunger is much simpler in its mechanical construction than the choke plungers used in standard waveguide. The only precaution that must be taken is that the plane of the piston be kept perpendicular to the axis of the circular waveguide for all axial positions of the piston.

It is of interest to examine the effect of a non-contacting short-circuiting plunger on other propagating modes. All propagating modes other than those of the circular-electric type have non-vanishing radial components of current at the gap.³ These radial currents excite the gap and are partially dissipated in the lossy material behind the plunger. The non-contacting piston is an excellent short-circuit for the circular-electric modes and, in addition, serves as a mode-filtering device to reduce the amplitudes of the lower-order propagating modes.⁴

Two non-contacting short-circuiting pistons were constructed. The generator piston contains a housing for the generator loop while the terminating piston is similar in construction with the exception that the loop housing is absent.

The method of varying the position of either short-circuiting piston is direct and distances can be measured accurately and rapidly. The position of the pistons can be varied individually over several guide wavelengths by long accurately machined micrometer screws. Distances as small as 0.0005

inch can be measured accurately by means of a gear-counter assembly.

Detecting Arrangement

The detector consists of four identical shielded loops similar to the exciting loop. These loops are uniformly spaced about the circumference with the loop axes oriented in the z direction. The loops are coplanar and oriented so that the currents excited on the loops are codirectional. These balanced shielded loops respond to the ϕ component of the surface current on the guide wall. By means of matching stubs, the individual outputs are adjusted to be in phase. The in-phase outputs are then connected together and to the input of a radio-frequency receiver.

A detector of this type is sensitive to the TE_{on} and $TE_{(3+k)n}$ modes (k is an integer). Investigation of the various modes capable of propagating in the 5.755 in. diameter tubing indicates that the effective wavelength of operation for the detector is from 8.636 to 11.985 cm. In the range from 7.158 to 8.636 cm. the detector will respond to the TE_{41} mode as well as the TE_{01} mode. It is observed, however, that measurements can be made in this range due to the damping effect on the TE_{41} mode caused by the lossy material behind the short-circuiting pistons.

The arrangement of the shielded loops in the generator and detector planes is shown in Fig. 5. A view of the generating loop and detecting loops as seen looking into the circular waveguide is shown in Fig. 6.

The Resonance-Curve Method

A transmission-line circuit which is representative of the waveguide circuit is shown in Fig. 7. In this diagram V_g is the equivalent generator and Z_g is the equivalent generator impedance. The distance w is the fixed distance between the load impedance and the detector. The total length of line l_1 is varied by moving the generator piston.

If a linear detector is used to measure the voltage at any position along the transmission line, the observed voltage is⁵

$$|V_1| = \left[\frac{|V_g|^2 (\sinh^2 \rho_g + \sin^2 \phi_g) (\sinh^2 \rho_1 + \cos^2 (\gamma_1 w + \phi_1))}{\sinh^2 (\rho_g + \rho_1) + \sin^2 (\gamma_1 l + \phi_g + \phi_1)} \right]^{\frac{1}{2}}$$

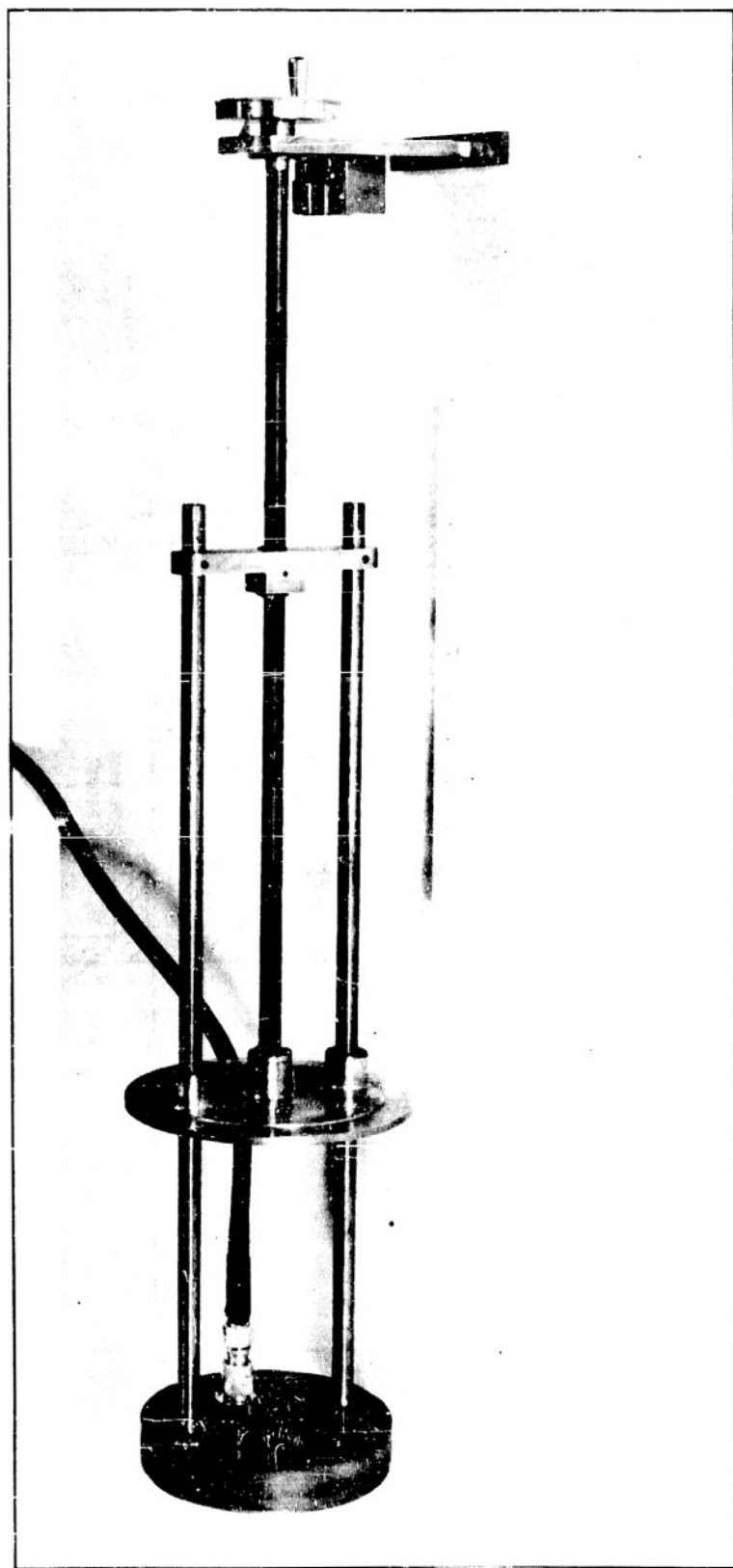


FIG. 3 GENERATOR PISTON

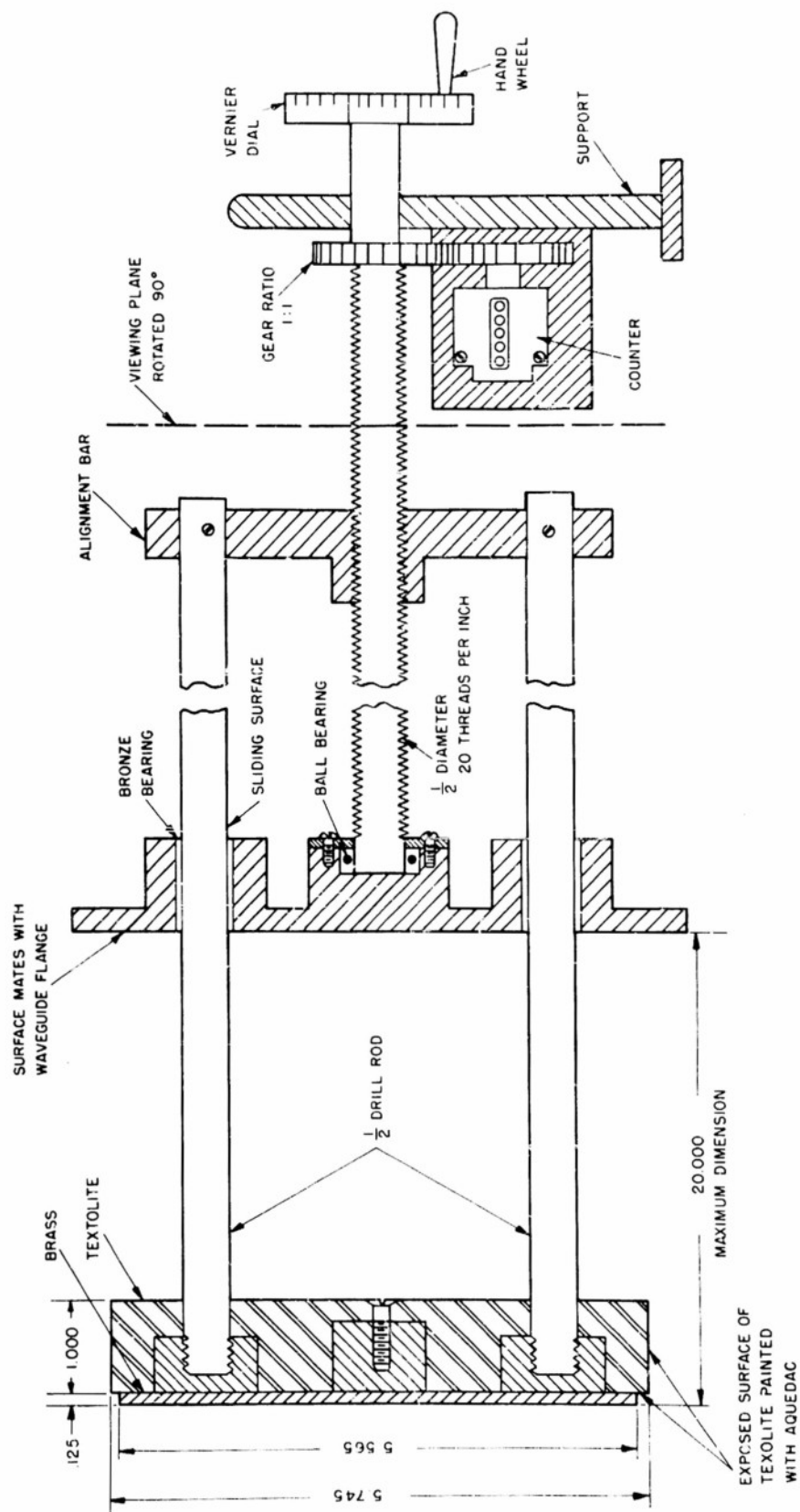


FIG. 4 ASSEMBLY DRAWING OF SHORT-CIRCUITING PISTON

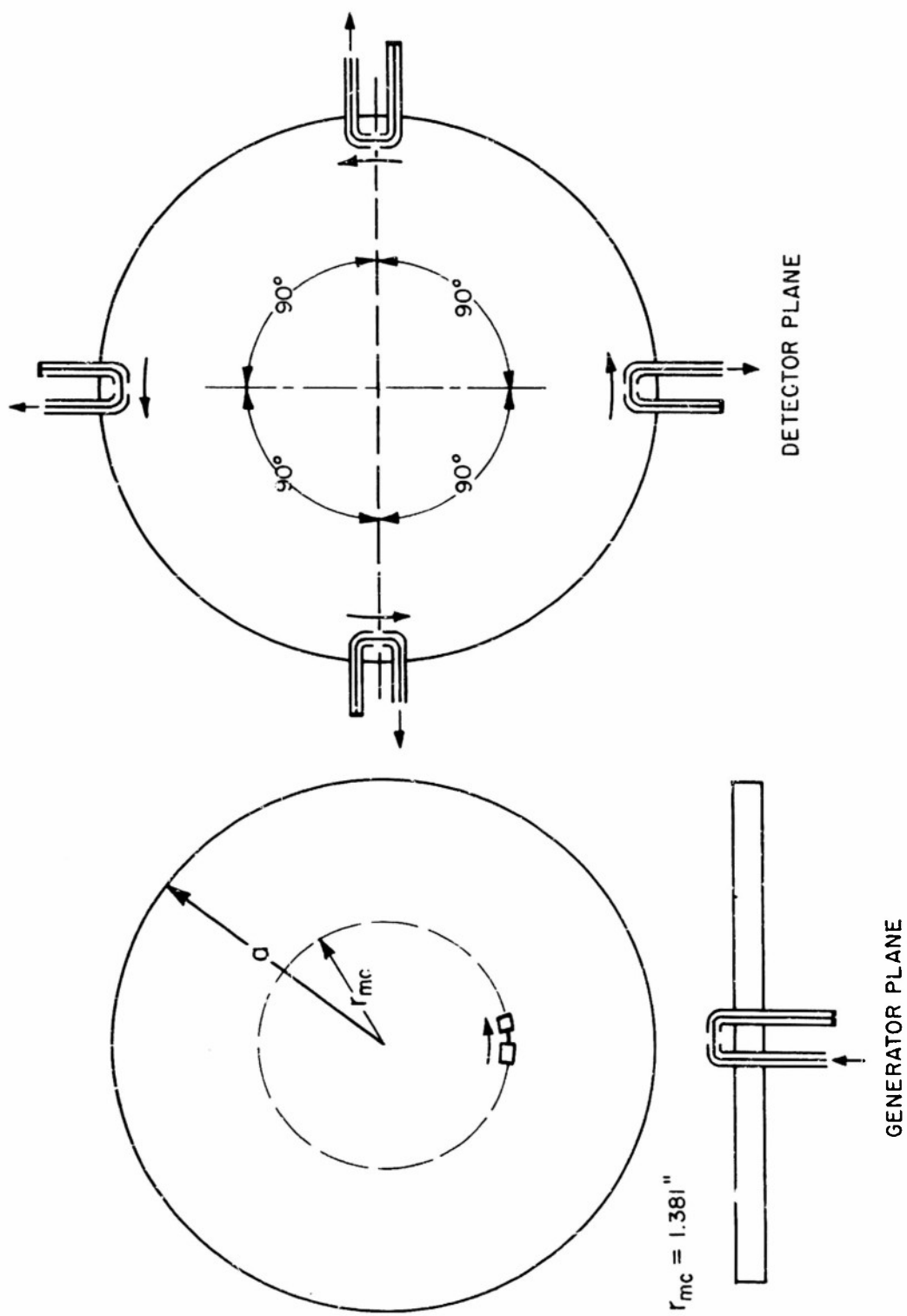


FIG. 5 ORIENTATION OF SHIELDED LOOPS IN THE DETECTOR AND GENERATOR PLANES
(NOT TO SCALE)



FIG. 6 VIEW OF DETECTING AND GENERATING LOOPS

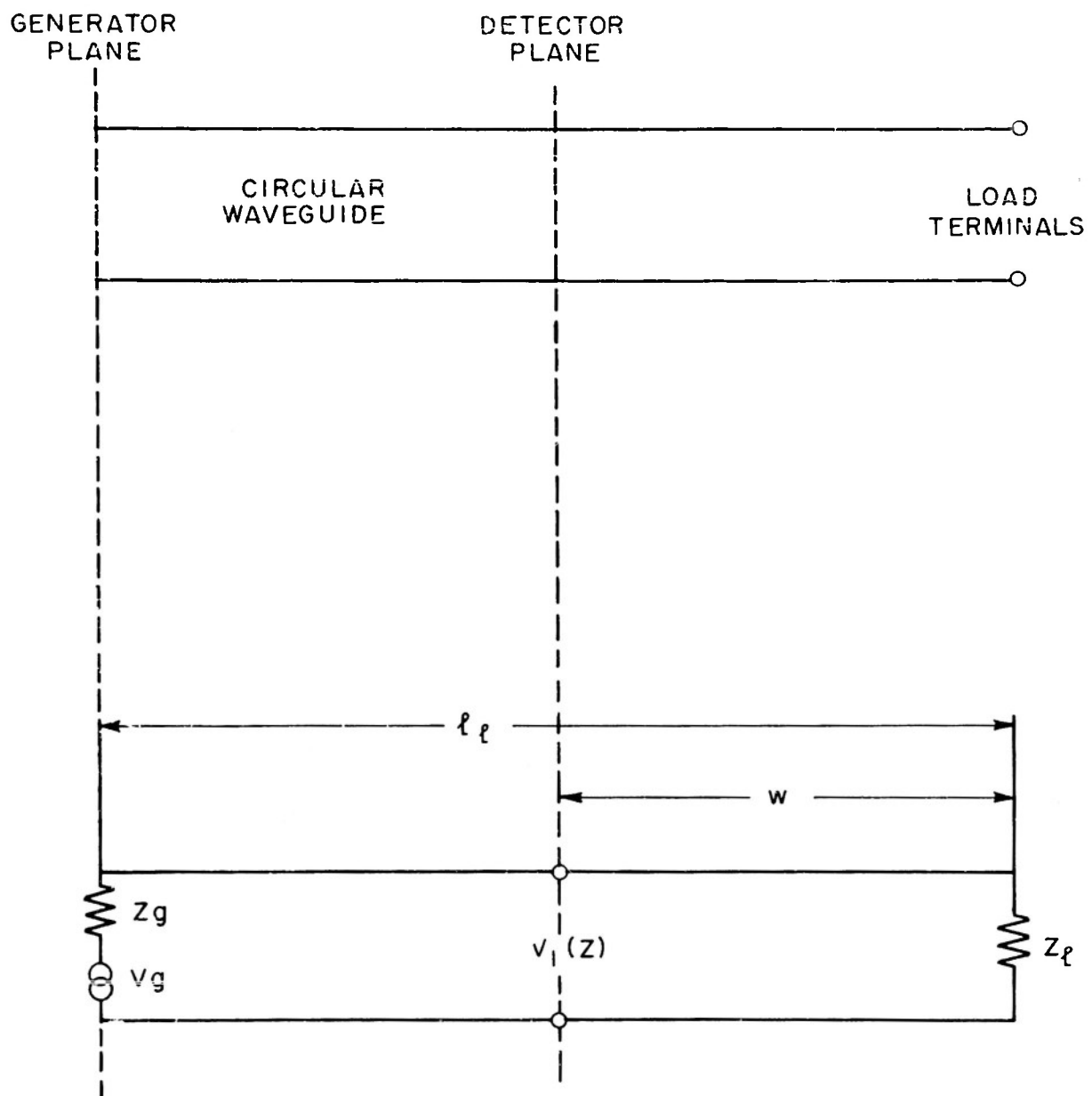


FIG. 7 EQUIVALENT TRANSMISSION LINE CIRCUIT

where it is assumed that the attenuation of the line can be neglected.

The normalized generator impedance and normalized load impedance are conveniently defined by

$$\left. \begin{aligned} \frac{Z_g}{Z_{cl}} &= \coth \theta_g = \coth (\rho_g + j\bar{\phi}_g) \\ \frac{Z_1}{Z_{cl}} &= \coth \theta_1 = \coth (\rho_1 + j\bar{\phi}_1) \end{aligned} \right\}$$

Since the line losses are known to be extremely small for the TE_{01} mode,⁶ the relation between the terminal functions ρ_1 and $\bar{\phi}_1$ and the resistance and reactance of the load are given by

$$\left. \begin{aligned} \frac{R_1}{R_{cl}} &= \frac{\sinh 2\rho_1}{\cosh 2\rho_1 - \cos 2\bar{\phi}_1} \\ \frac{X_1}{R_{cl}} &= \frac{-\sin 2\bar{\phi}_1}{\cosh 2\rho_1 - \cos 2\bar{\phi}_1} \end{aligned} \right\}$$

The terminal function can be obtained readily from

$$\rho_1 = \sinh^{-1} \left(\sin \gamma_1 \frac{W}{Z} \right)$$

where W is the width of the resonance curve measured between the half power points.

For load terminations which have little loss

$$\rho_1 \simeq \gamma_1 \frac{W}{Z}$$

$\bar{\phi}_1$ is determined by comparison with a standard termination $\bar{\phi}_{st}$. If a short-circuit ($\bar{\phi}_{st} = \pi/2$) is used as a standard termination, then

$$\bar{\phi}_1 = \frac{\pi}{2} + \gamma_1 (l_{st} - l_1)$$

provided that the same maximum or minimum is used for both standard and unknown terminations. In the previous equation l_{st} is the total resonant length of line with a standard termination and l_1 is the resonant line length with the unknown termination.

It is customary to use the standing-wave-ratio in plotting data on the Smith Chart. The relationship between the terminal function ρ_1 and the voltage-standing-wave-ratio S is given by

$$S = \coth \rho_1$$

A loosely coupled generator and loosely coupled detector are assumed.

Radio-Frequency Signal Source

The radio-frequency signal source is a McNally Tube Generator which was originally designed at the Radio Research Laboratory by Mr. William Huggins and subsequently used by Dr. Seymour Cohn.⁷ This oscillator has been modified to use a RK 707B reflex klystron instead of a 2K28 tube for which it was originally designed. The 1000 cycle-per-second square-wave modulator was also modified by the author to insure negligible frequency modulation in the oscillator output. The frequency range of the oscillator is from 1200 to 5900 megacycles-per-second with an average power output of approximately 10 milliwatts.

Radio-Frequency Receiver

A superheterodyne receiver is used to detect the output of the detecting loops to insure high sensitivity and linearity in detection. The receiver is a SPR/2 type of receiver designed to detect signals in the 1000 to 10,000 megacycle-per-second frequency range. The output of this receiver is connected to a Ballantine vacuum-tube voltmeter through a 1000 cycle-per-second filter. The receiver output was calibrated by the usual method of comparing a sine wave distribution with the distribution on a slotted line terminated in a short-circuit. A calibration curve of the over-all detecting system is shown in Fig. 8.

Procedure for Making Impedance Measurements

A block diagram of the experimental arrangement used in making imped-

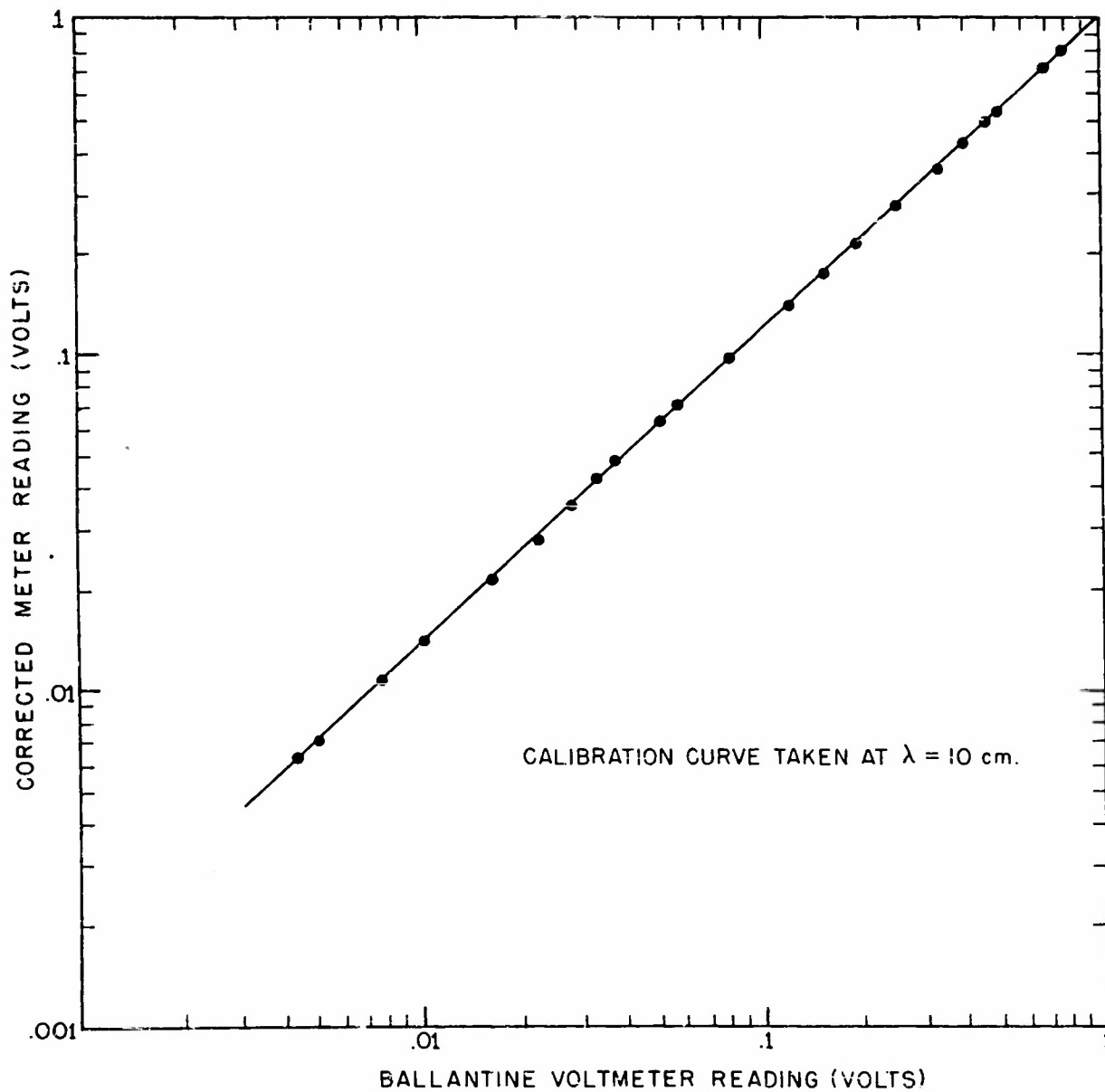


FIG. 8 CALIBRATION CURVE OF AN/SPR-2 RECEIVER

ance measurements on the TE_{01} transmission line is shown in Fig. 9. A photograph of the experimental setup is shown in Fig. 10,

After a period of two hours for stabilization, the oscillator is set to the desired frequency. A spectrum analyzer (model TSS-4SE) is used to properly tune the oscillator and to monitor the output power level of the McNally tube oscillator. The free space wavelength is measured by a coaxial wavemeter (model TFS-5). The detected output of the wavemeter is amplified by a bolometer amplifier whose output terminals are connected to a Ballantine voltmeter.

Once the correct frequency has been obtained, the output transmission lines of the detecting loops are tuned for maximum sensitivity to the TE_{01} mode. This is accomplished by terminating the circular waveguide with a short-circuit which can be varied in position. The waveguide terminated in a short-circuit can be regarded as a cavity. The fields corresponding to the normal modes are only slightly perturbed by the presence of the shielded loops, and the resonant-guide wavelengths correspond to those of the normal modes. By observing the modal spectrum, the tuning stubs in the detector assembly are adjusted to obtain maximum sensitivity for the desired circular-electric mode.

The tuning arrangement is shown in Fig. 11. Several cables of supposedly equal lengths were made up and their electrical lengths compared. The method of comparison consists of adjusting the length of circular waveguide until a TE_{11} resonance occurs. The monitoring loop is used as the detector in this measurement. With the cavity in resonance the outputs of two oppositely located shielded loops are led through the test cables to a standard T section. The output of the T is then connected to the receiver. If the cable lengths are identical electrically, the receiver indication will be zero. This procedure is repeated until 4 cables are found that are suitable. This proper choice of cables makes the detector insensitive to the TE_{11} and TE_{31} modes.

By connecting the output cables through tuning stubs as in Fig. 11 the problem of tuning is simplified to tuning out the TE_{21} mode. This can be accomplished by varying the output plunger over several half-

wavelengths and observing the detector output. Typical tuning curves are given in Fig. 12. The upper graph shows the resonance response when the detecting loops are properly tuned. In this case the response of the TE_{01} mode is observed to be at least 38 db above all extraneous modes. In the lower graph the resonance response as the terminating plunger is varied is given for the stubs in a detuned position. It is observed that the TE_{21} response is 16 db down from that of the desired TE_{01} mode. It is also observed that the TE_{11} and TE_{31} modes are absent.

The TM_{11} mode and the TE_{01} mode are degenerate modes; i.e., these modes have the same cutoff wavelengths. To identify positively the circular-electric mode a monitoring loop is mounted on the circular waveguide wall. The monitoring loop is similar to the previously described shielded loops except that a suitable scale is provided for angular rotation of the monitoring loop. A photograph of the monitoring shielded loop is shown in Fig. 13. A coaxial line-stretcher serves as a rotary joint and allows the rapid rotation of the monitoring loop about its axis.

The TE_{01} mode has purely transverse wall currents while the TM_{11} mode is characterized by solely longitudinal wall currents. The output of the monitoring loops as a function of angle of rotation is a sensitive test for distinguishing between the two degenerate modes, when the cavity is resonant in a TE_{01n} mode.

If θ_r is the angle of rotation of the monitoring loop from the theoretical angular position of maximum surface current for the circular-electric wave, then, if a pure TE_{01} wave exists, the output due to the desired mode will be proportional to $\cos \theta_r$. If the TM_{11} mode is also present, then the output will be proportional to $A \cos \theta_r + B \sin \theta_r$. It is apparent that $|A|$ is the amplitude of the TE_{01} surface current and $|B|$ is the amplitude of the TM_{11} surface current at the particular point of measurement. The ratio of $|B|$ to $|A|$ is obtained immediately by setting the loop at $\theta_r = 0$ degrees and determining the amplitude $|A|$, and then setting the loop to $\theta_r = 90$ degrees and obtaining the amplitude $|B|$. The output versus rotation characteristics of a cavity resonant in the TE_{01} mode is given in Fig. 14. The results indicate that the generator loop is properly oriented and only the TE_{01} mode

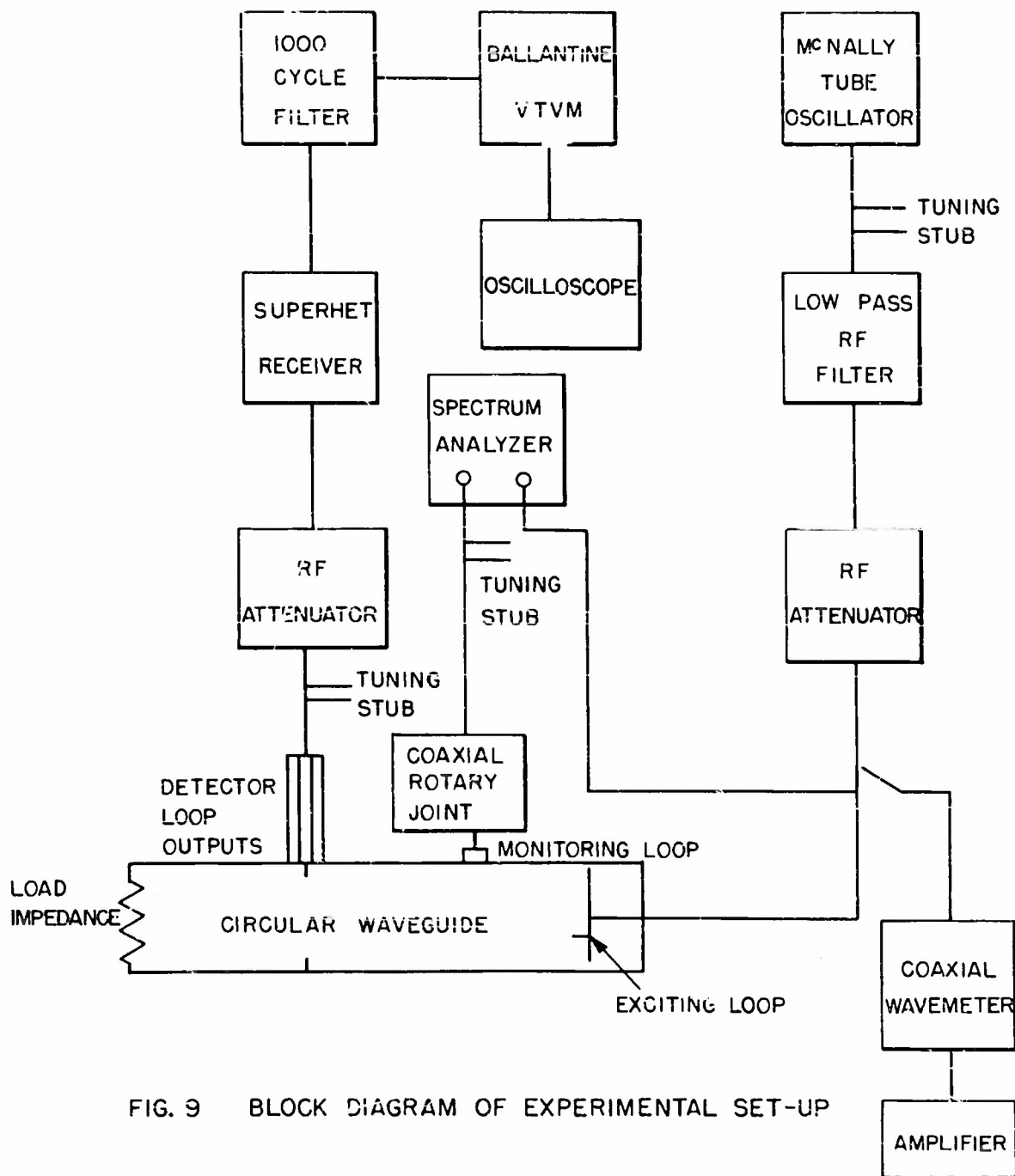


FIG. 9 BLOCK DIAGRAM OF EXPERIMENTAL SET-UP

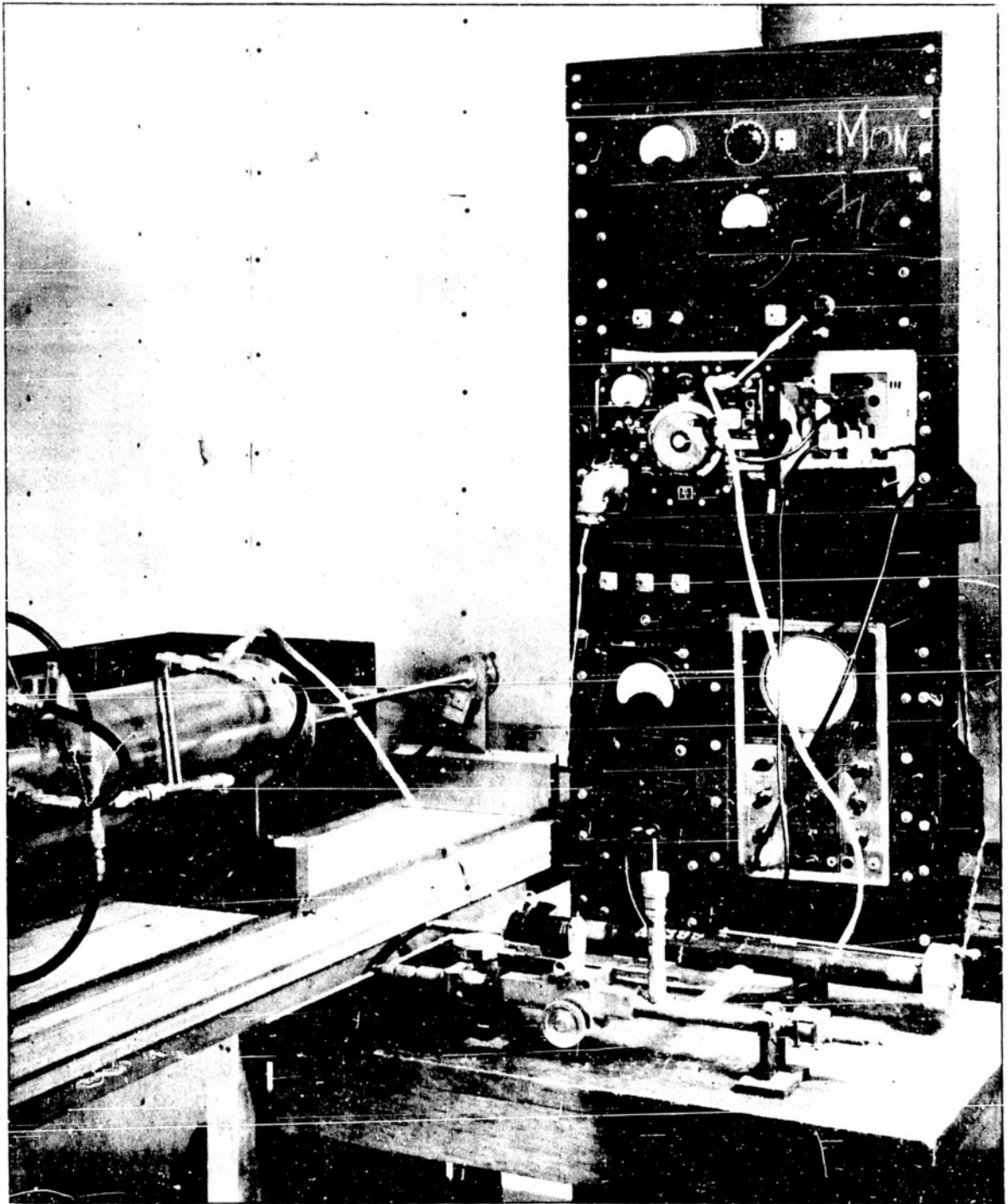


FIG. 10 EXPERIMENTAL ARRANGEMENT FOR MEASUREMENTS
ON " TE_{01} TRANSMISSION LINE"

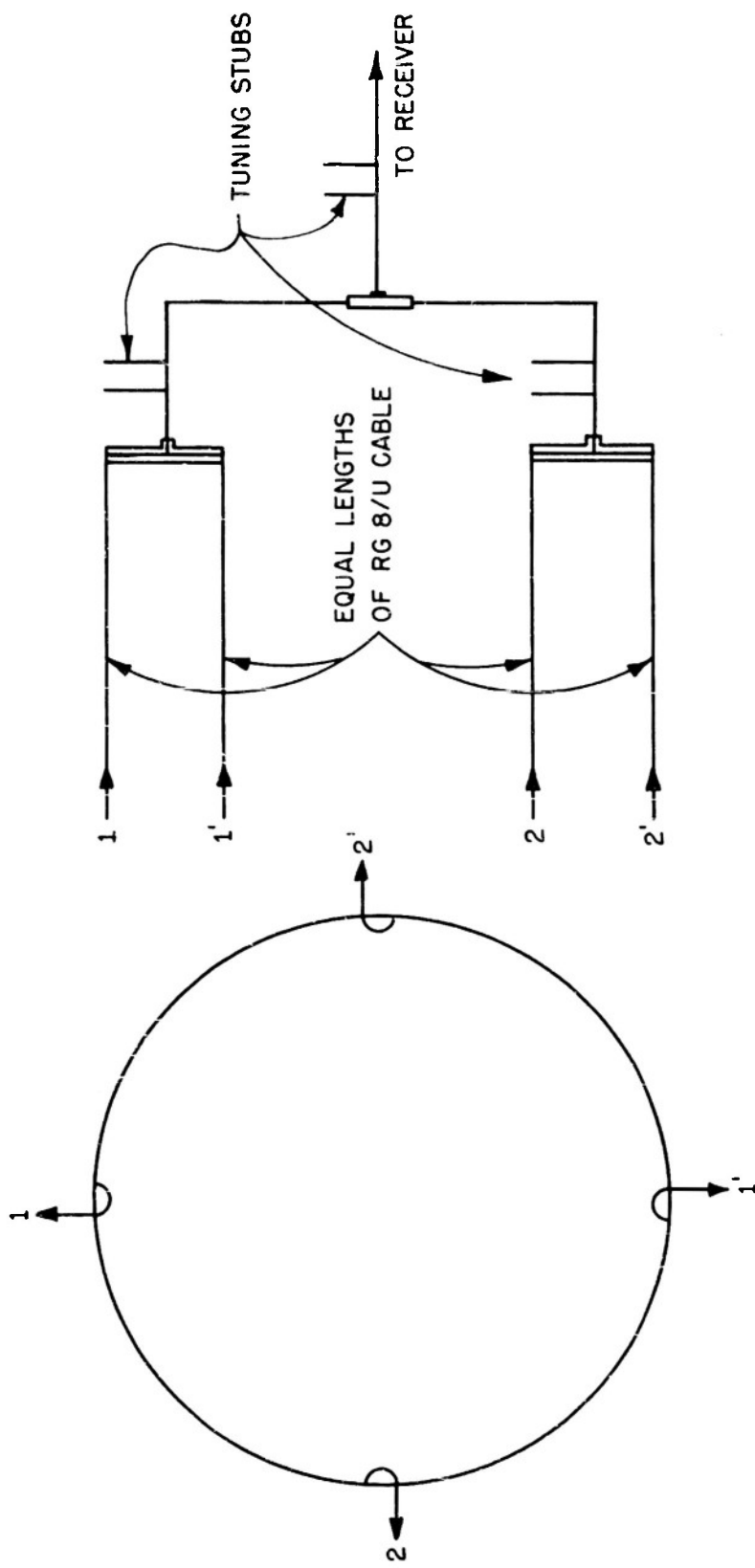


FIG. 11 ARRANGEMENT FOR TUNING DETECTOR

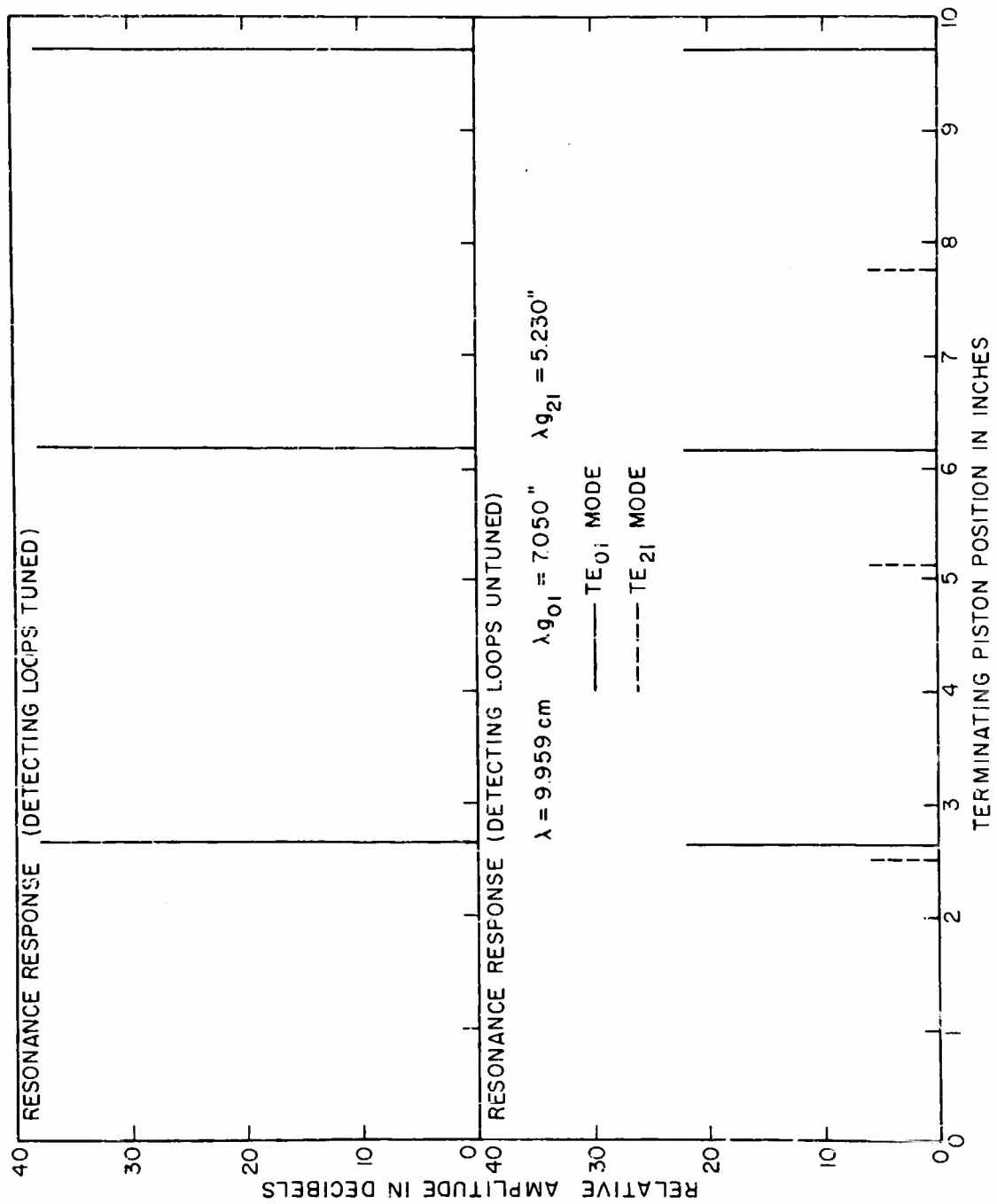


FIG. 12 DETECTOR OUTPUT AS A FUNCTION OF POSITION OF SHORT-CIRCUITING PISTON

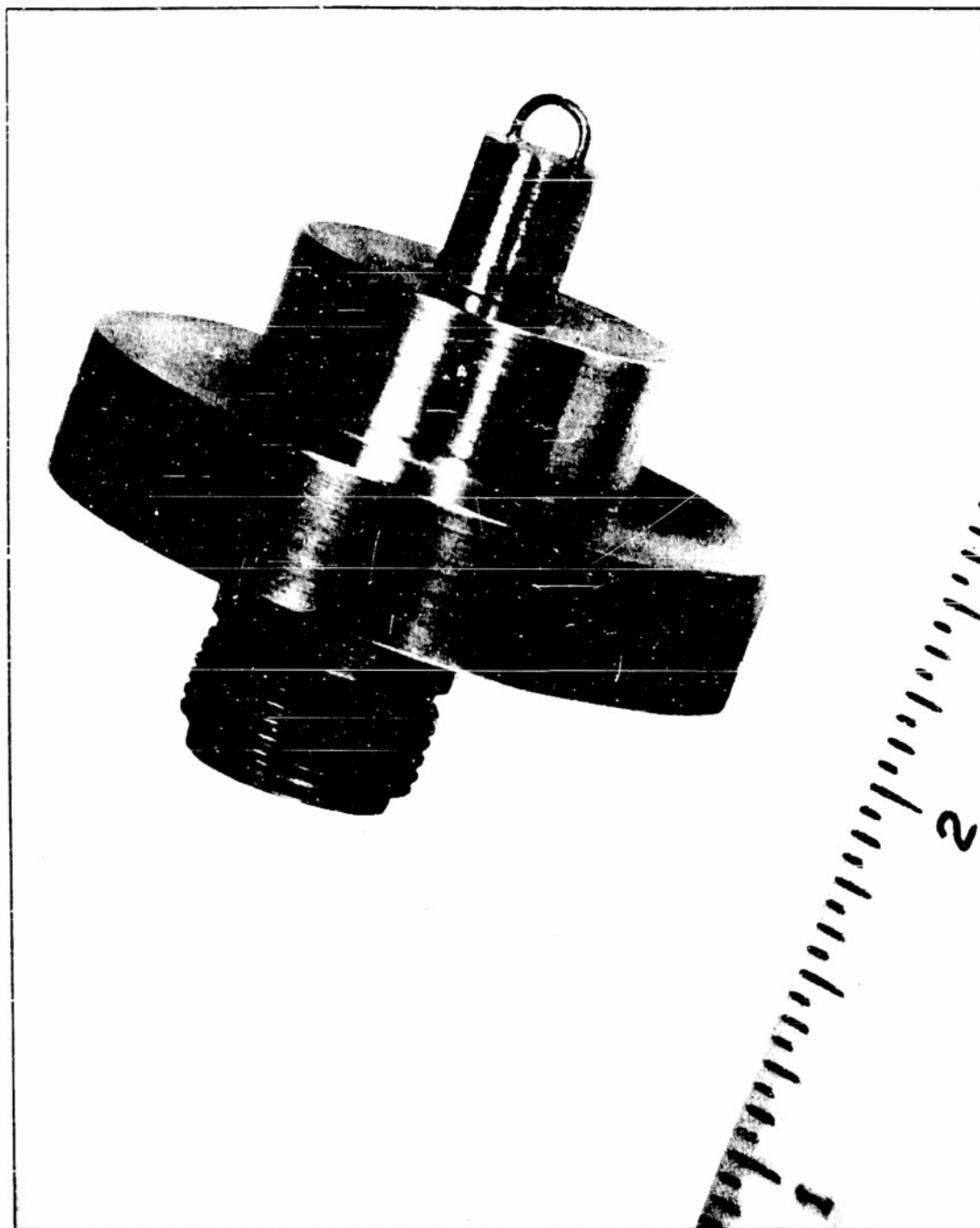


FIG. 13 MONITORING LOOP

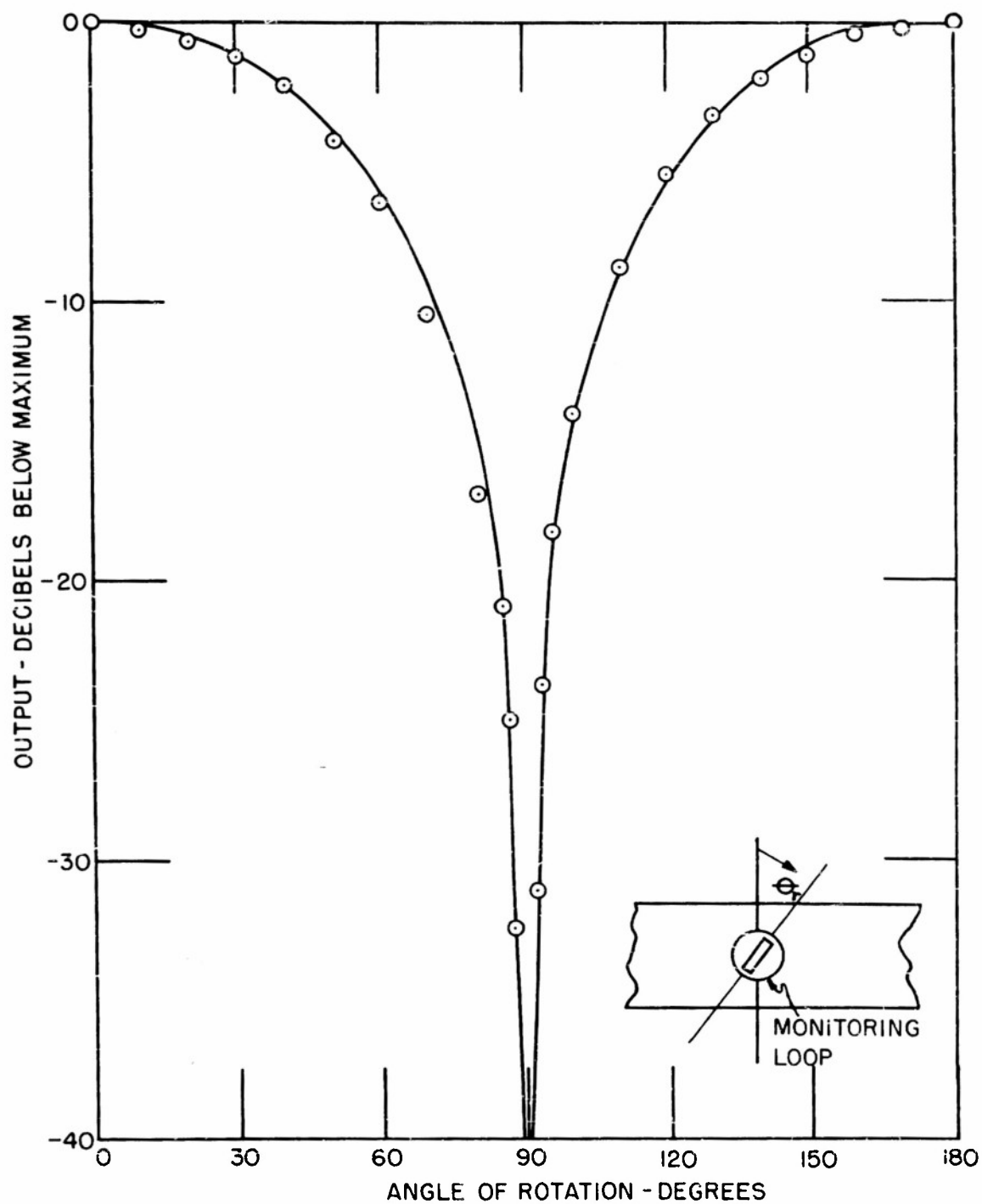


FIG. 14 OUTPUT OF MONITORING LOOP AS A FUNCTION OF ANGLE OF ROTATION

is excited. It is also observed that the monitoring loop has a high degree of balance.

Once the oscillator is properly tuned and sufficiently padded, and the detector output matched to the receiver, impedance measurements can be made in the circular waveguide.

Load Terminations

Due to the inherent symmetry of the circular-electric mode, the nature of the loads is restricted to those having circular symmetry. This restriction is readily understandable because a sharp deviation from circular symmetry would result in modal conversion to other propagating modes. Modal conversion would effectively increase the attenuation and no advantage would be obtained by using the circular-electric mode.

In case a matched load is desired, a long conical section constructed from lossy material should serve the purpose adequately. In all situations where precise measurements of junction characteristics are desired, a matched termination is not required provided that a good short circuit can be obtained.

One of the corrections that must be made in making precise impedance measurements on the conventional transmission line is due to finite losses in the line itself as well as losses in the short circuit. This correction can be neglected when making measurements in a circular waveguide supporting a TE_{01} wave because of its low transmission losses. To illustrate the quality of the short circuit a typical resonance curve taken with the circular waveguide resonant in the TE_{018} mode is shown in Fig. 15.

II.

MEASUREMENT OF THE NORMALIZED SUSCEPTANCE OF A CIRCULAR OBSTACLE

Open-Circuit Method of Measuring Shunt Susceptance

The simplest way to measure shunt susceptance on a transmission-line is to insert a quarter wavelength of short-circuited line in parallel with the susceptance to be measured. If the reference plane is chosen at the plane

of the thin lossless obstacle, the normalized admittance is given directly by

$$\frac{Y}{Y_{cl}} = \frac{-jB}{Y_{cl}} = j \cot \gamma_1 (l_1 - l_{st})$$

$$|\gamma_1 (l_1 - l_{st})| < \frac{\pi}{2}$$

where l_{st} is the total resonant length of line with a short circuit at the plane of the obstacle and l_1 is the resonant line length with the obstacle inserted in the obstacle mount and the short circuit located $\lambda g/4$ behind the obstacle.

This type of measurement requires that the obstacle be thin and planar. In addition, it is necessary for the transmission line and the short circuiting piston to have extremely low losses. If an ideal short circuit is unavailable, a simple correction can be made which compensates for the finite impedance of the quarter wavelength of short circuited line.

The experimental arrangement for the measurement of a planar obstacle in a circular waveguide excited by an incident TE_{01} wave is shown in Fig. 16. In order to cover a considerable frequency band, measurements were made at $\lambda = 7.321$ cm., $\lambda = 8.150$ cm., $\lambda = 9.737$ cm., and $\lambda = 10.441$ cm.

The circular obstacles were fabricated from flat brass stock of 0.016 in. thickness. Extreme care was taken to maintain concentricity in cutting the aperture in the solid sheeting. The obstacle thickness t in terms of guide wavelength is given below.

a/λ	λ cm. calculated	λg cm. measured	$t/\lambda g$
0.70	10.441	21.262	.00191
0.75	9.737	16.700	.00243
0.90	8.150	11.110	.00366
1.00	7.321	9.245	.00440

Ten circular obstacles were fabricated with values of $\delta = 0.50, 0.55,$

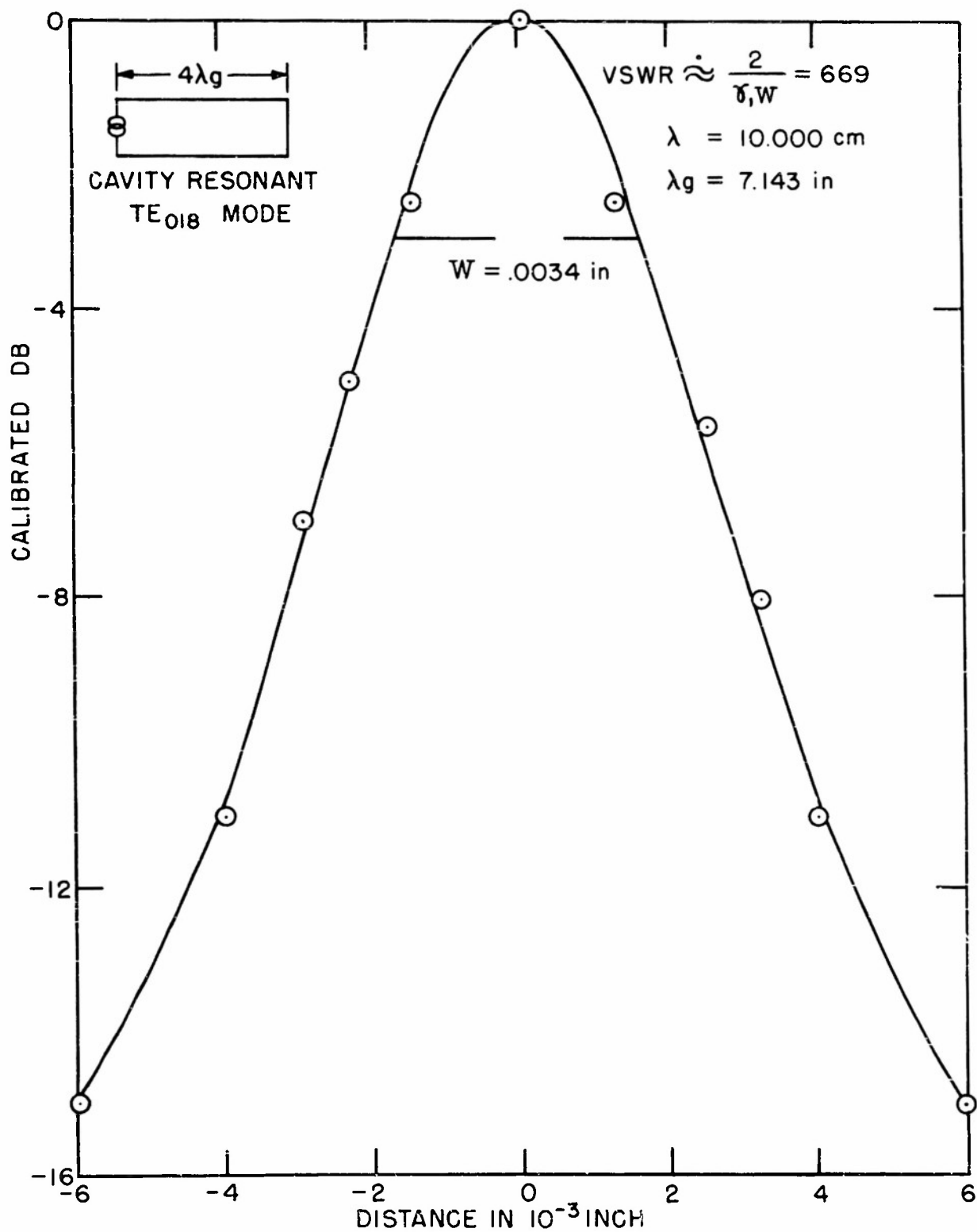
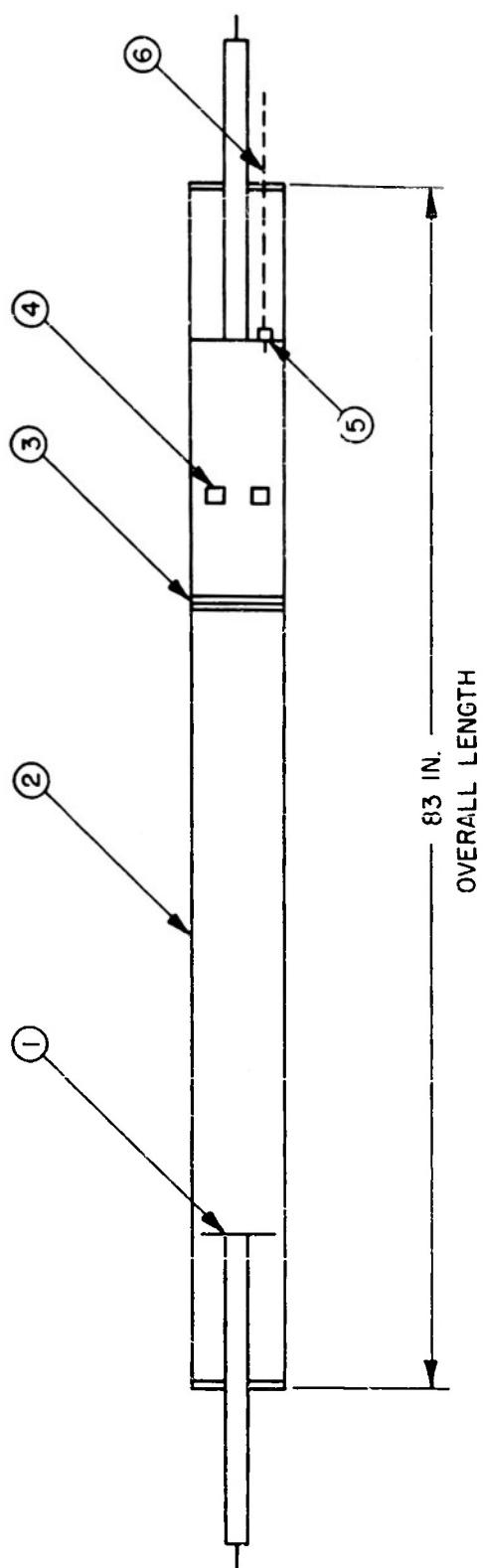


FIG. 15 A TYPICAL RESONANCE CURVE



- ① TERMINATING SHORT-CIRCUITING PISTON
- ② BRASS TUBING 5.755 IN. I.D. 0.125 IN. WALL
- ③ FLANGE-TYPE OBSTACLE MOUNT
- ④ DETECTING ASSEMBLY
- ⑤ GENERATOR LOOP AND GENERATOR SHORT-CIRCUITING PISTON
- ⑥ RG 8/U CABLE

FIG. 16 EXPERIMENTAL ARRANGEMENT FOR MEASURING THE SUSCEPTANCE OF
A THIN OBSTACLE

0.60, 0.65, 0.70, 0.75, 0.80, 0.85, 0.90, 0.95. A photograph of the obstacles and the flange-type mount is shown in Fig. 17.

The precise measurement of obstacle susceptance by the open-circuit method depends to a great extent on locating the reference position correctly. In order to locate the short circuit accurately, an aperture-less obstacle is inserted in the obstacle mount. With a short circuit at the obstacle plane, the generator is then moved at least 4 half-wavelengths and the positions of the various resonances observed. The guide wavelength is then calculated by averaging the readings of the difference between the consecutive resonance positions. The obstacle is then inserted into the mount and the terminating piston is set at a distance of $\lambda_g/4$ from the reference plane of the obstacle. The shift in the resonance position is observed and the normalized susceptance is then calculated.

Sample Calculation

To obtain an idea of the accuracy of measurement, consider the typical set of experimental data obtained in the measurement of a circular obstacle with $\delta = 0.70$ and $a/\lambda = 0.75$.

(l_1) c.u.	(l_{st}) c.u.	$(l_{st} - l_1)$ c.u.
332.773	343.619	10.846
267.075	277.917	10.842
201.360	212.203	10.843
135.638	146.511	10.873

$$10.851 \text{ c.u.} = (l_{st} - l_1) \text{ av.}$$

The data are given in counter-units where 1 counter-unit (c.u.) corresponds to an axial distance of 0.050 in. *

The guide wavelength if measured to be

$$\lambda_g = 6.571 \text{ in.} = 16.690 \text{ cm.}$$

*Since the difference $(l_{st} - l_1)$ is required, it is not necessary to know the exact distances corresponding to l_{st} and l_1 .

and the normalized susceptance is calculated from

$$\frac{B}{Y_{cl}} = \cot \gamma_1 (l_{st} - l_1) = 1.754$$

or in a more convenient form

$$\frac{B}{Y_{cl}} \frac{a}{\lambda g} = 0.767$$

Theoretical and Experimental Results

Calculated and measured values of obstacle susceptance for δ (aperture to guide radius ratio) between 0.5 and 1.0 are given in Fig. 18. The theoretical values were obtained by a variational principle.⁸ It is observed that $B/Y_{cl} \cdot a/\lambda g$ is plotted against δ with a/λ as a parameter. The experimental data has been taken over a wavelength range from 7.40 to 11.40 cm. and is seen to be in excellent agreement with the theoretical results. These curves can be used to obtain the susceptance of a circular obstacle providing the obstacle meets the requirements set forth by the theory.

Conclusion

The small discrepancy between experimental and theoretical results can be attributed to

1. Approximate nature of the theory.
2. Finite thickness of the obstacle.
3. Finite conductivity of obstacle and waveguide.
4. Presence of unwanted modes.
5. Difficulty in keeping the thin obstacle planar.
6. Ellipticity of the circular waveguide.
7. Slight asymmetry of the obstacle aperture with respect to the guide axis.
8. Typical errors involved in the measurement of admittance by the resonance curve method.

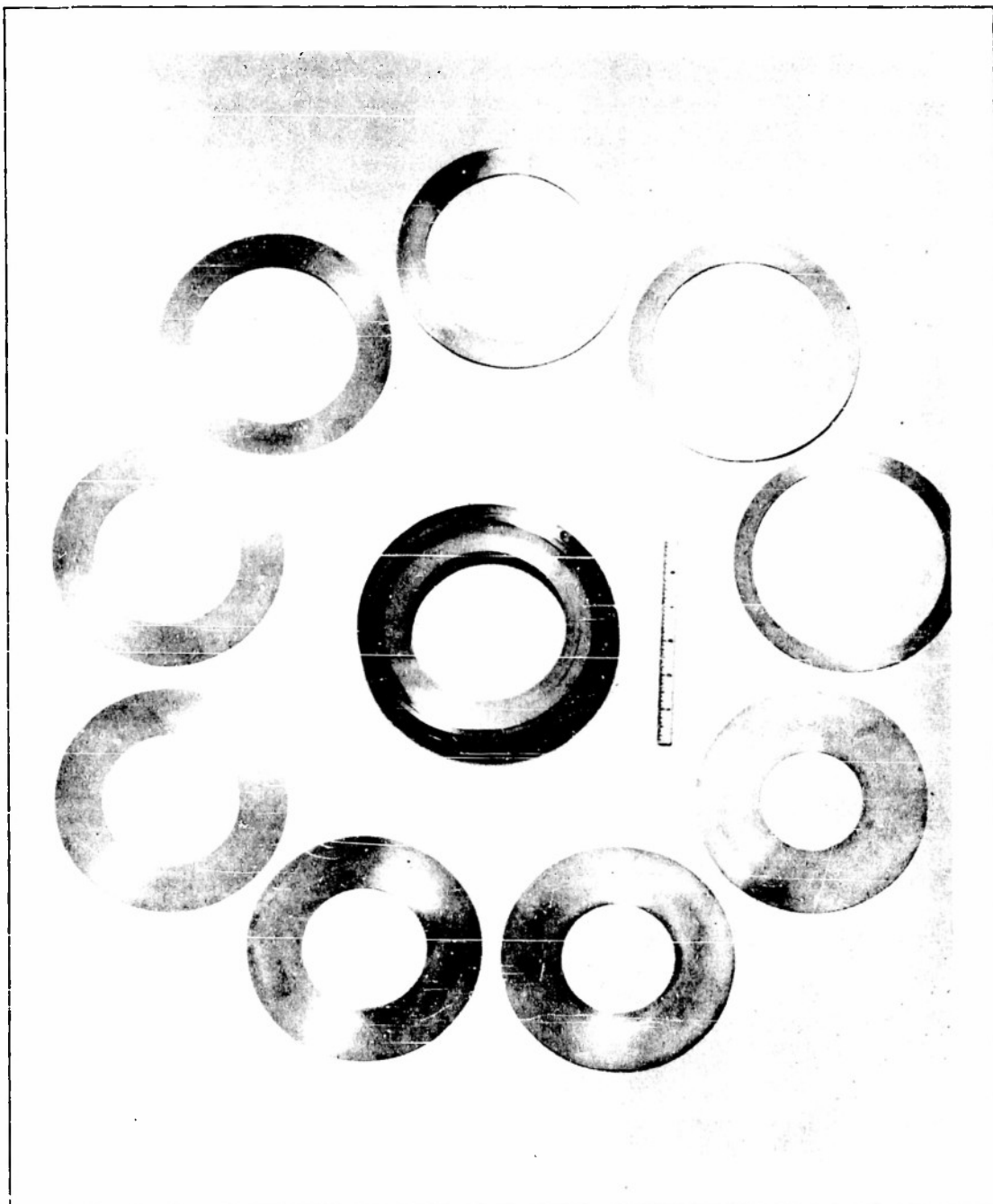


FIG.17 PHOTOGRAPH OF OBSTACLES AND FLANGE-TYPE MOUNT

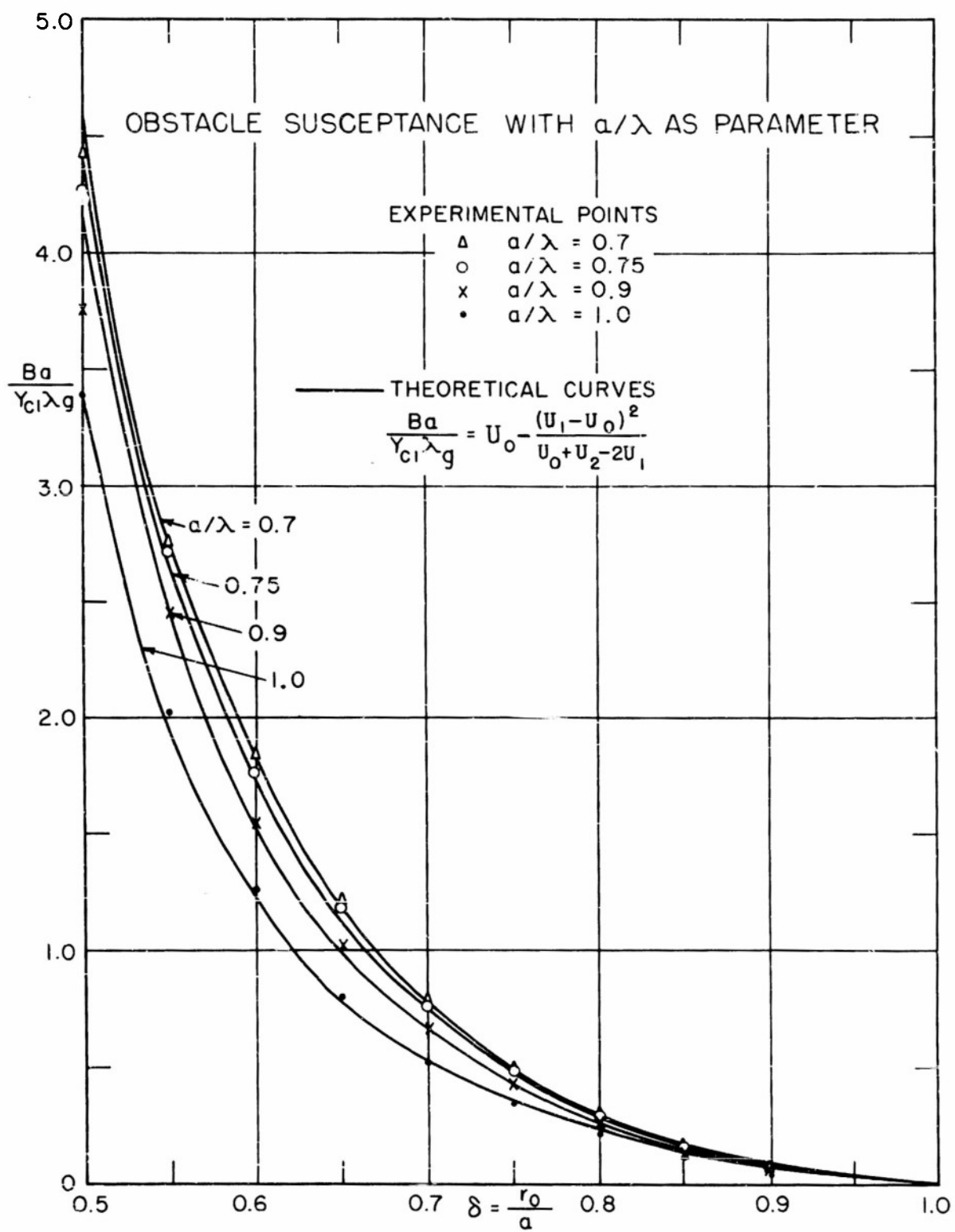


FIGURE 18

III.

EXPERIMENTAL DETERMINATION OF THE ELEMENTS OF
THE SCATTERING MATRIX OF A CIRCUMFERENTIAL GAP

The elements of the scattering matrix of a circumferential gap in a circular waveguide supporting the TE_{01} mode are obtained by Deschamps' graphical method for analyzing waveguide junctions. It is assumed that the dominant circular-electric is the only propagating mode in the 5.755 in. i.d. brass tubing. Measurements are made of junctions with gap widths up to 1.750 in. at a free space wavelength of 10.000 cm. A detailed description of the measurement procedure is given. The experimental results are found to be in excellent agreement with the theory.

The mode filtering properties of the circumferential gap are observed by comparing the power radiated by the gap when excited respectively by a unit TM_{01} wave and a unit TE_{01} wave.

Description of Experimental Arrangement for the Measurement
of the Scattering Matrix of a Circumferential Gap.

The experimental setup for the measurement of the gap parameters is similar to the one described in the previous sections. In order to introduce the circumferential gap in the wall of the circular waveguide, two additional sections of tubing are used as shown in the photograph of Figure 19. Each of these sections is tapered externally to a sharp edge to insure physical boundary conditions similar to those considered in the theoretical aspect of the problem, i.e., that the guide walls are infinitely thin.⁹

The setting of the gap width to a specific dimension is facilitated by using as a gauge a precisely milled aluminum bar with a rectangular cross-section. Four aluminum bars with cross sectional dimensions $1/8" \times 1/4"$; $1/4" \times 1/2"$; $1/2" \times 1"$; and $1" \times 2"$ are used to adjust gap widths in $1/8"$ steps. The tolerances of the dimensions of these standard bars are ± 0.001 in.

The entire waveguide structure is kept cylindrical by mounting the waveguide on aluminum blocks. Each block has two machined grooves so

that the waveguide assembly can slide along brass alignment tracks. The alignment tracks consist of $1/2'' \times 1/2''$ brass bars which are screwed to the 1.5 in. thick plywood base. Set screws permit the waveguide to be clamped in any position along the track. Once the gap width is set, the set screws keep the waveguide components in position insuring that the gap width does not change during measurement of the scattering parameters. All measurements of gap characteristics were made at $\lambda = 10,000$ cm.

Typical Measurement Procedure (For gap width of 1.750 in.)

Prior to actual measurement of the scattering matrix elements by Deschamps' method, it is convenient to define the input and output terminals of the circumferential gap. These reference terminal planes are chosen as in Fig. 20. The input reference position is obtained by placing a short circuit at the input terminals and observing the resonance response by moving the generator piston. Two resonance positions are observed to check the guide wavelength and one of these positions is chosen as the input reference terminals. With the generator piston in a position of resonance, the short circuit is removed from the input terminals and the gap is closed ($2g = 0$). The terminating short circuit is then moved and two consecutive resonances recorded. One of these positions is chosen as the output reference terminals.

Once the reference planes are located, the gap width is set to the desired dimension. For this typical example the gap width is set to 1.750 in. The impedance at the input terminals is measured with the short circuiting plunger at the following positions of $\gamma_1 l$: $0, \pi/8, \pi/4, 3\pi/8, \pi/2, 5\pi/8, 3\pi/4, 7\pi/8$; where $\gamma_1 l = 0$ corresponds to a short circuit at the output terminals ($\Gamma = 1e^{-j\pi}$) and $\gamma_1 l = \pi/2$ represents an open circuit at the output terminals ($\Gamma = 1$).

Instead of only four data points, eight points are taken in order to determine quickly an estimate of the experimental errors involved. The positions of the short circuiting piston are equally spaced along a half-wavelength in the output line so as to insure a good distribution of data.

Determination of Elements of Scattering Matrix

by Deschamps' Graphical Method $2g = 1.750$ in.

The experimental values of the measured impedance at the input termi-

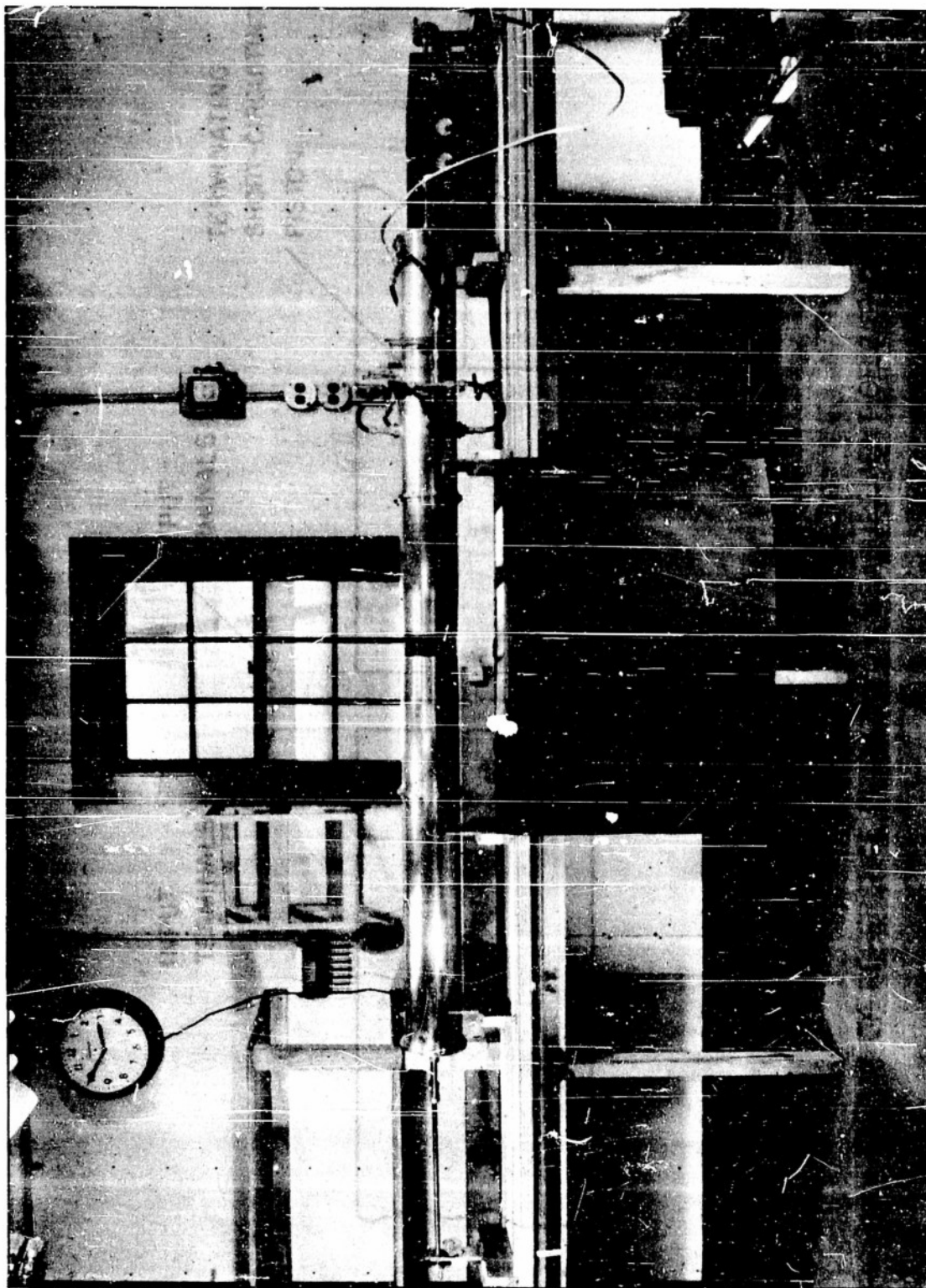


FIG. 19 EXPERIMENTAL ARRANGEMENT FOR MEASUREMENT OF THE SCATTERING MATRIX
OF A CIRCUMFERENTIAL GAP

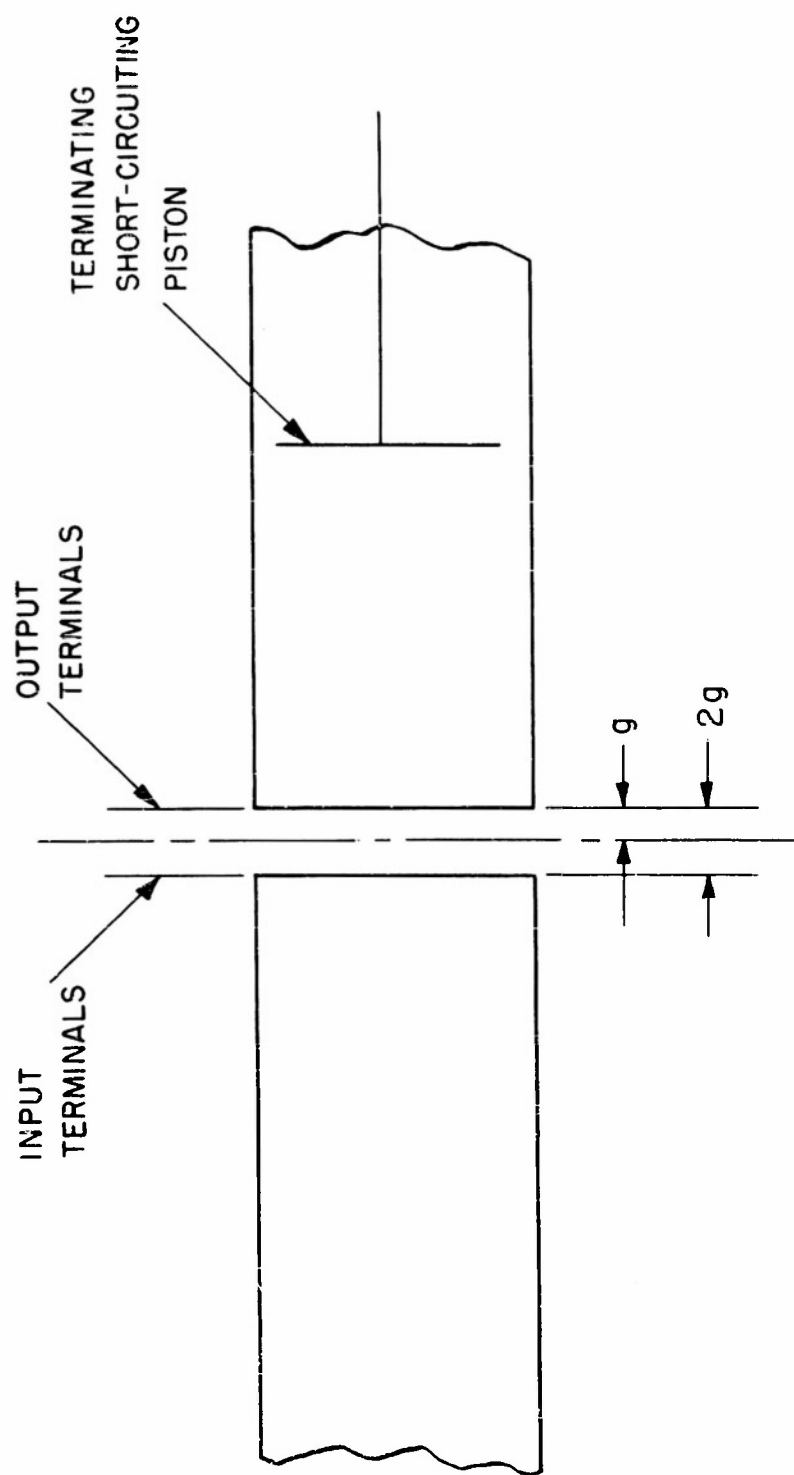


FIG. 20 CHOICE OF REFERENCE PLANES FOR MEASUREMENT OF GAP CHARACTERISTICS

nals of the junction are plotted on the Smith Chart of Fig. 21 for the indicated positions of the short circuiting piston in the output circuit. Since the constructions are to be carried out in the reflection-coefficient plane, it is advisable to use a Smith Chart with superimposed reflection-coefficient circles. Obviously, since the accuracy of the results depends on the accuracy of the constructions, for precision measurements an enlarged reflection-coefficient chart should be used.

Corresponding pairs of data points for $\gamma_{11} = (0, \pi/2)$, $(\pi/8, 5\pi/8)$, $(\pi/4, 3\pi/4)$, and $(3\pi/8, 7\pi/8)$ are joined by straight lines and the nature of the intersection observed. Theoretically, these chords should intersect in the crossover point S'_{11} . Owing to experimental error, they may not; and the quality of their intersection is a measure of the consistency of the experimental data. Thus if the four lines intersect in the manner shown in the enlarged view of the crossover region in Fig. 22, there is an indication of an error in one of the two measurements associated with what appears to be a "bad" chord, i.e., for the short circuiting piston at either $\gamma_{11} = \pi/8$ or $\gamma_{11} = 5\pi/8$. Since two extra pairs of points have been taken, it appears reasonable to disregard this one line and take S'_{11} at the center of the tiny triangle formed by the other three lines. This analysis of the data can be performed directly after the readings are taken, and the data plotted on the reflection coefficient chart.

In a previous report¹⁰ it has been indicated that all measured points should lie on a circle of center C' . If the center of the circle is to be found by the intersection of the perpendicular bisectors of the various chords, a similar situation is encountered as in determining the crossover point. Again only the six reliable points are used, and an appropriate center C' for the circle is chosen at the center of the triangle. Finally, the circle is drawn with an average radius determined by measuring the distances from C' to the measured points and averaging these distances. It is now apparent that the point corresponding to $\gamma_{11} = \pi/8$ is in error, probably owing to the fact that the particular standing-wave measurement was partially masked by noise.

Now that S'_{11} and C' have been found and the circle G' drawn, graphical constructions are performed to determine the amplitudes of the scat-

tering matrix elements, as shown in Fig. 23. All the graphical constructions could be made in the combined Smith-reflection-coefficient chart, but, since the constructions actually refer to the reflection-coefficient plane, only the coordinate lines of this plane need be used to illustrate the required constructions. For three-place accuracy, a reflection coefficient chart of one meter in diameter was used. The values obtained for the amplitudes of the elements of the scattering matrix for a gap width of 1.750 in. are

$$|S_{11}| = \overline{OS_{11}} = 0.331$$

$$|S_{12}| = \frac{\overline{S_{11}E^r}}{\sqrt{r}} = 0.808$$

$$|S_{22}| = \frac{\overline{S_{11}C^r}}{r} = 0.328$$

Since the junction is known to be symmetrical, $|S_{11}|$ should be equal to $|S_{22}|$. The results obtained are in good agreement, considering that the distances are only measurable within 0.001 units. In most cases knowledge of the amplitudes $|S_{11}|$, $|S_{12}|$, and $|S_{22}|$ is all that is desired, and the simple construction of Fig. 23 is sufficient to calculate the division of power due to the presence of the junction. Thus, if this junction were terminated in a matched load, the percentage of power reflected would be

$$\% \text{ Power reflected} = |S_{11}|^2 \times 100\% = 10.96\%$$

Similarly, the percentage of power transmitted through the junction to a matched load is

$$\% \text{ Power transmitted} = |S_{12}|^2 \times 100\% = 65.29\%$$

and the percentage of power dissipated in the junction is

$$\% \text{ Power dissipated} = (1 - |S_{11}|^2 - |S_{12}|^2) \times 100\% = 23.75\%$$

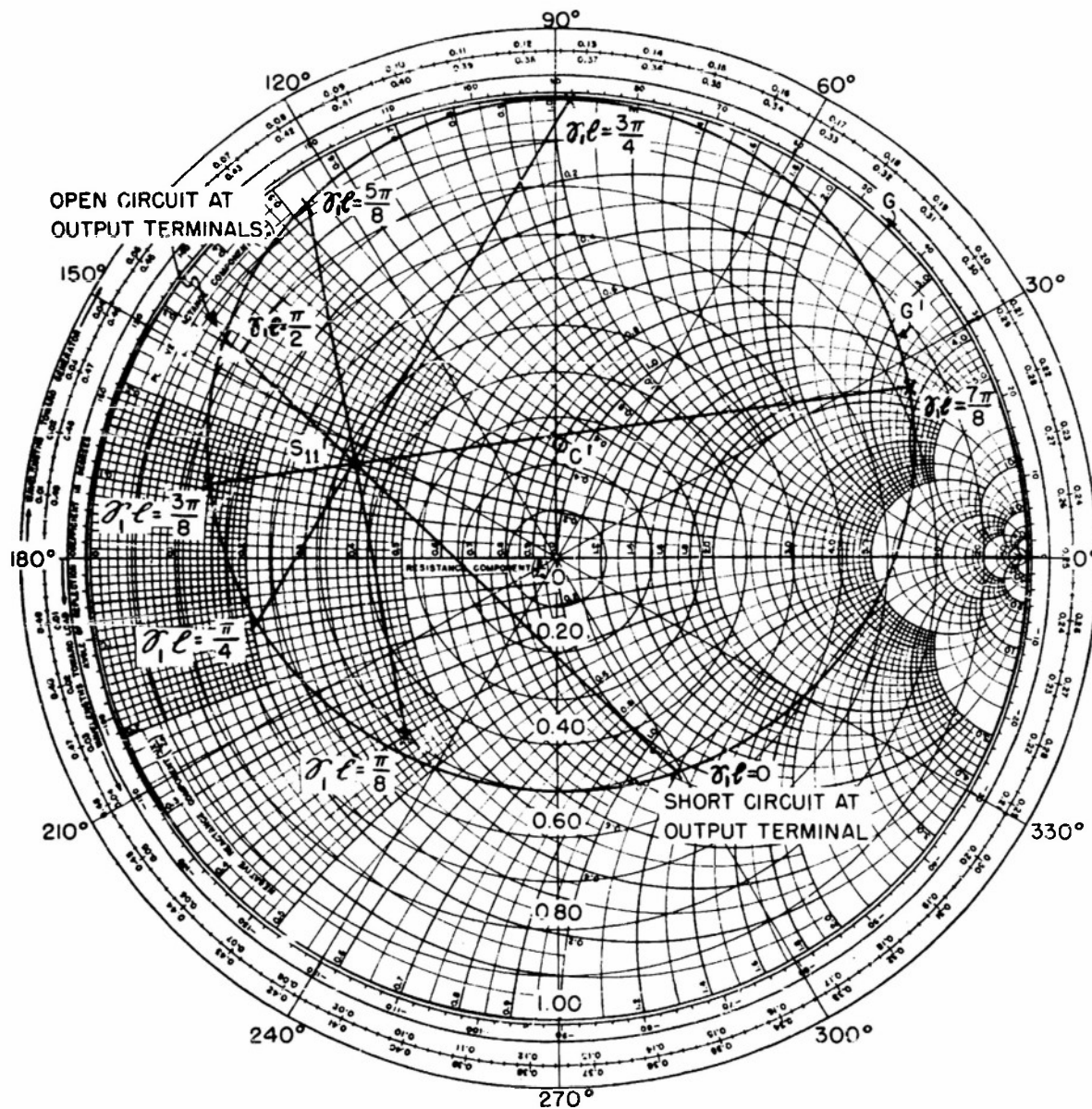


FIG. 21 EXPERIMENTAL DATA PLOTTED ON SMITH - REFLECTION COEFFICIENT CHART AND CONSTRUCTIONS FOR LOCATING S_{11}' AND C'

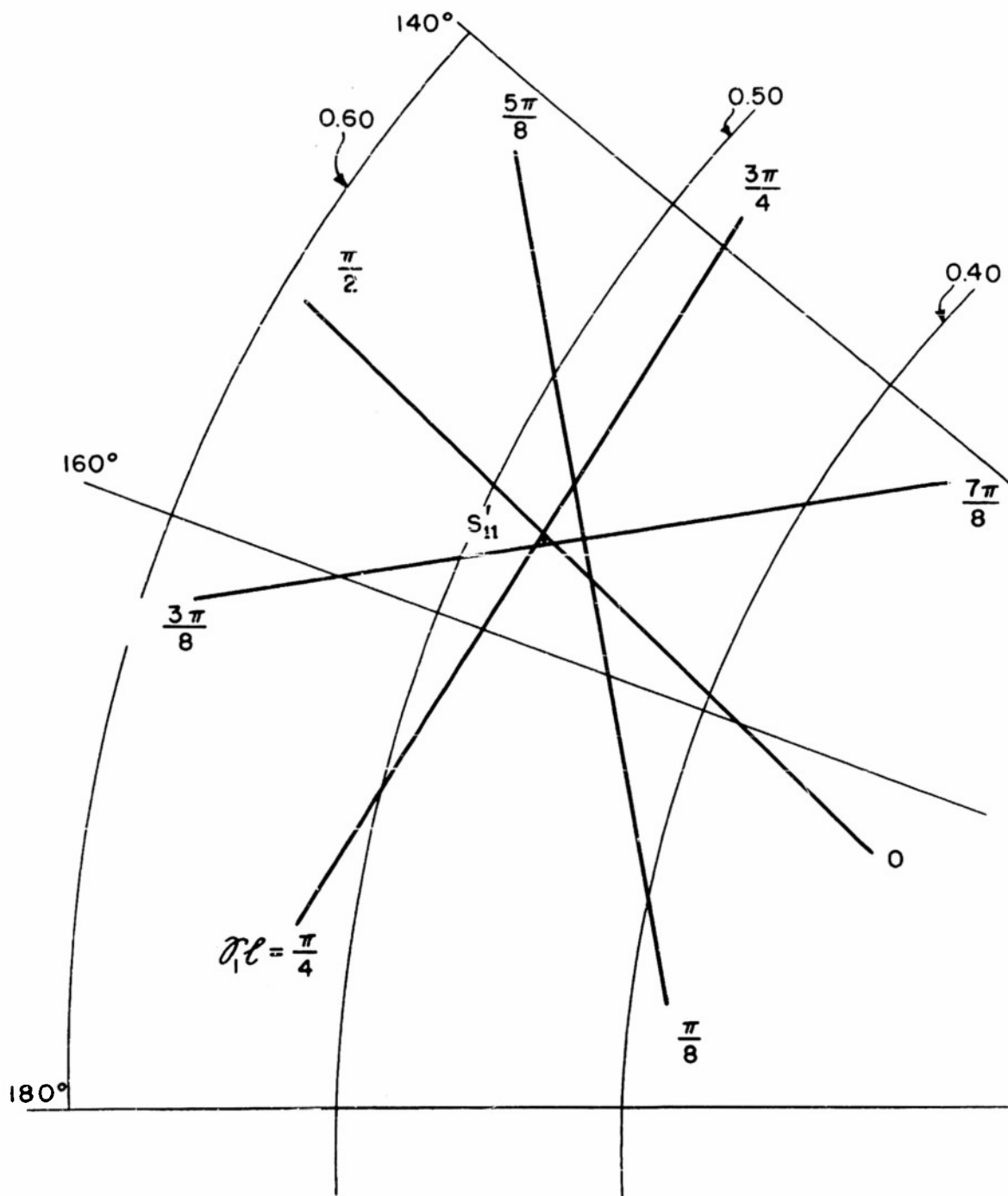


FIG. 22 ENLARGED VIEW OF CROSS-OVER REGION

$$|S_{11}| = \overline{OS_{11}} = .331$$

$$|S_{12}| = \frac{\overline{S_{11}E'}}{\sqrt{r}} = .808$$

$$|S_{22}| = \frac{\overline{S_{11}C'}}{r} = .328$$

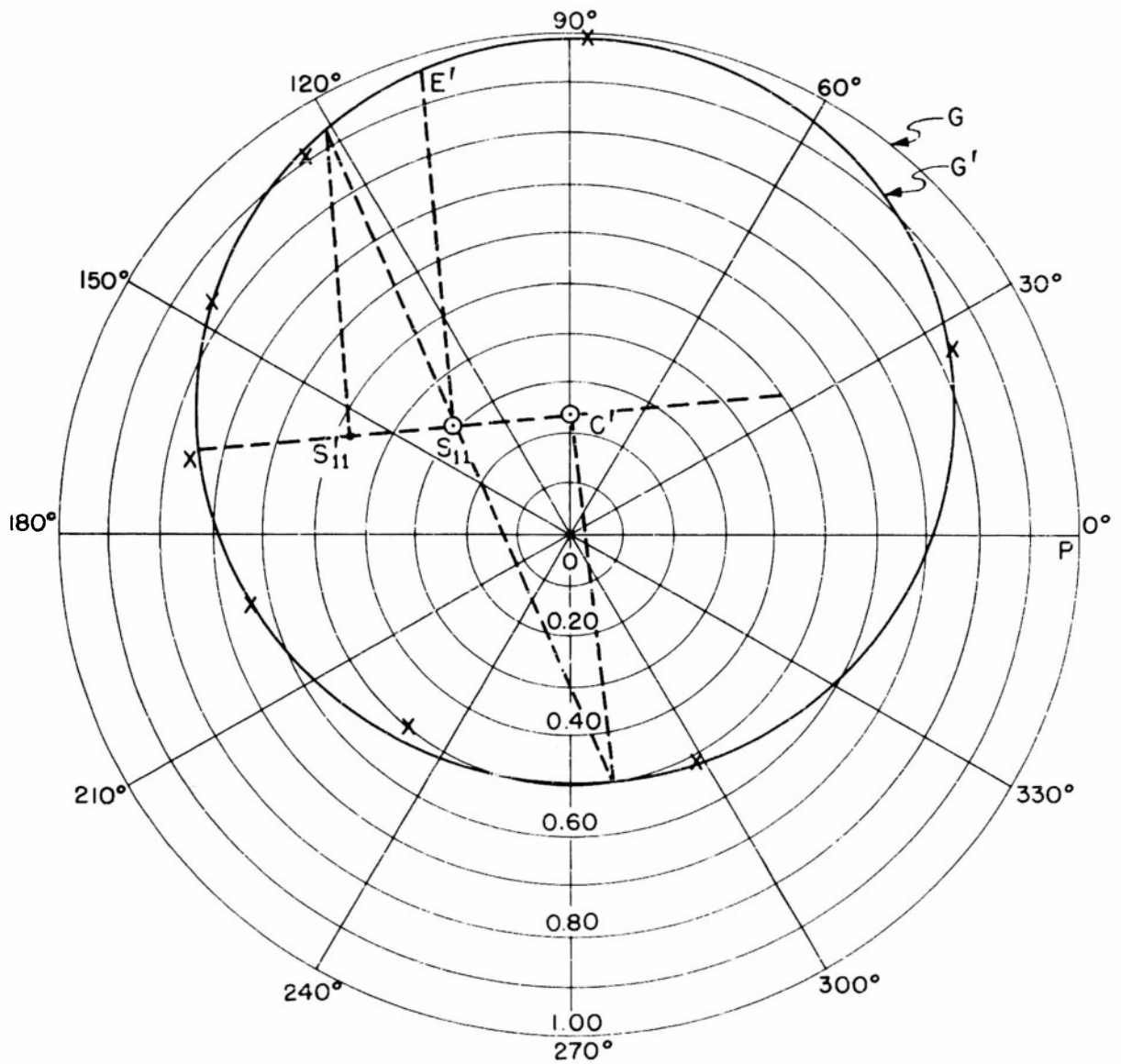


FIG. 23

GRAPHICAL DETERMINATION OF AMPLITUDES OF SCATTERING MATRIX ELEMENTS

If one wishes to introduce a matching network to eliminate the reflected power, it is necessary to know the phase of S_{11} . If it is also necessary to determine the equivalent circuit of the junction, then, the phase angles of all the scattering elements must be known. Fig. 24 illustrates the graphical construction required to find the phases of the elements of the scattering matrix. It is observed that all angles are measured in the conventional sense (positive if counterclockwise, negative if clockwise). The scattering matrix for a circumferential gap of 1.750 in. is thus determined to be

$$\| S \| = \begin{vmatrix} 0.331 \epsilon^{j135^\circ} & 0.808 \epsilon^{j70.6^\circ} \\ 0.808 \epsilon^{j70.6^\circ} & 0.328 \epsilon^{j132.8^\circ} \end{vmatrix}$$

The constructions of amplitude and phase have been performed separately to illustrate clearly the simple geometry required for the determination of each of these quantities. In practice, all the constructions could be performed on the same reflection-coefficient chart, and with experience many of the constructed lines could be omitted.

Equivalent T-Network Representation

If the junction is known to be symmetrical, the impedance elements of an equivalent T-section are given by

$$\text{Series arm} \quad Z_1 = \frac{1 + (S_{11} - S_{12})}{1 - (S_{11} - S_{12})}$$

$$\text{Shunt Arm} \quad Z_2 = \frac{2S_{12}}{(1 - S_{11})^2 - S_{12}^2}$$

Prior to the evaluation of the impedance elements, it is desirable to shift the reference planes located at the input and output terminals of the junction to the plane located at the center of the gap. This transformation is accomplished by multiplying each element of the scattering matrix by $\epsilon^{\frac{j4\pi g}{\lambda}}$ where g has been defined as the distance from the junction center to either the output or input terminals.

For this gap, $\frac{4\pi g}{\lambda g} = 88.2$ electrical degrees, and the transformation gives

$$\|S\|_{\text{trans.}} = \begin{vmatrix} 0.331 \epsilon^{j223.2^\circ} & 0.808 \epsilon^{j158.8^\circ} \\ 0.808 \epsilon^{j158.8^\circ} & 0.328 \epsilon^{j221.0^\circ} \end{vmatrix}$$

for the transformed scattering matrix.

In the evaluation of the expressions for Z_1 and Z_2 , it is possible to find two equally valid representations for the T-network, depending on the choice of the phase of S_{12} . Recalling that there is an indeterminacy of 180° in the graphical determination of this phase, one settles the ambiguity by choosing the phase of S_{12} to give positive values of resistance for the impedance elements of the T-section.

Carrying out the computations for the elements of the T-section, results in*

	$(S_{12} = 0.808 \epsilon^{j158.8^\circ})$	$(S_{12} = 0.808 \epsilon^{-j21.2^\circ})$
Z_1	$0.947 - j2.034$	$0.000 + j0.036$
Z_2	$-0.473 + j1.035$	$0.473 + j1.035$

These results indicate that it is necessary to add 180 degrees to the measured phase of S_{12} if one desires to obtain an equivalent T-section containing positive resistances.

An Additional Note on Deschamps' Method

During the experimental determination of the elements of the scattering matrix by Deschamps' graphical method, an additional check on the accuracy of the results was obtained by plotting the loci of S'_{11} , S_{11} , and C' as shown in Fig. 25. Since these loci should be continuous, smooth curves, an incorrect choice of S'_{11} or C' would cause these points to

*In performing these calculations the average value of the measured S_{11} and S_{22} is used for S_{11} in the equations for Z_1 and Z_2 .

$$\text{Arg } S_{11} = \angle (\overrightarrow{OP}, \overrightarrow{OS_{11}}) = 135^\circ$$

$$\text{Arg } S_{12} = \frac{1}{2} \angle (\overrightarrow{OP}, \overrightarrow{C'P_3''}) = 70.6^\circ$$

$$\text{Arg } S_{22} = \angle (\overrightarrow{S_{11}C'}, \overrightarrow{C'P_3''}) = 132.8^\circ$$

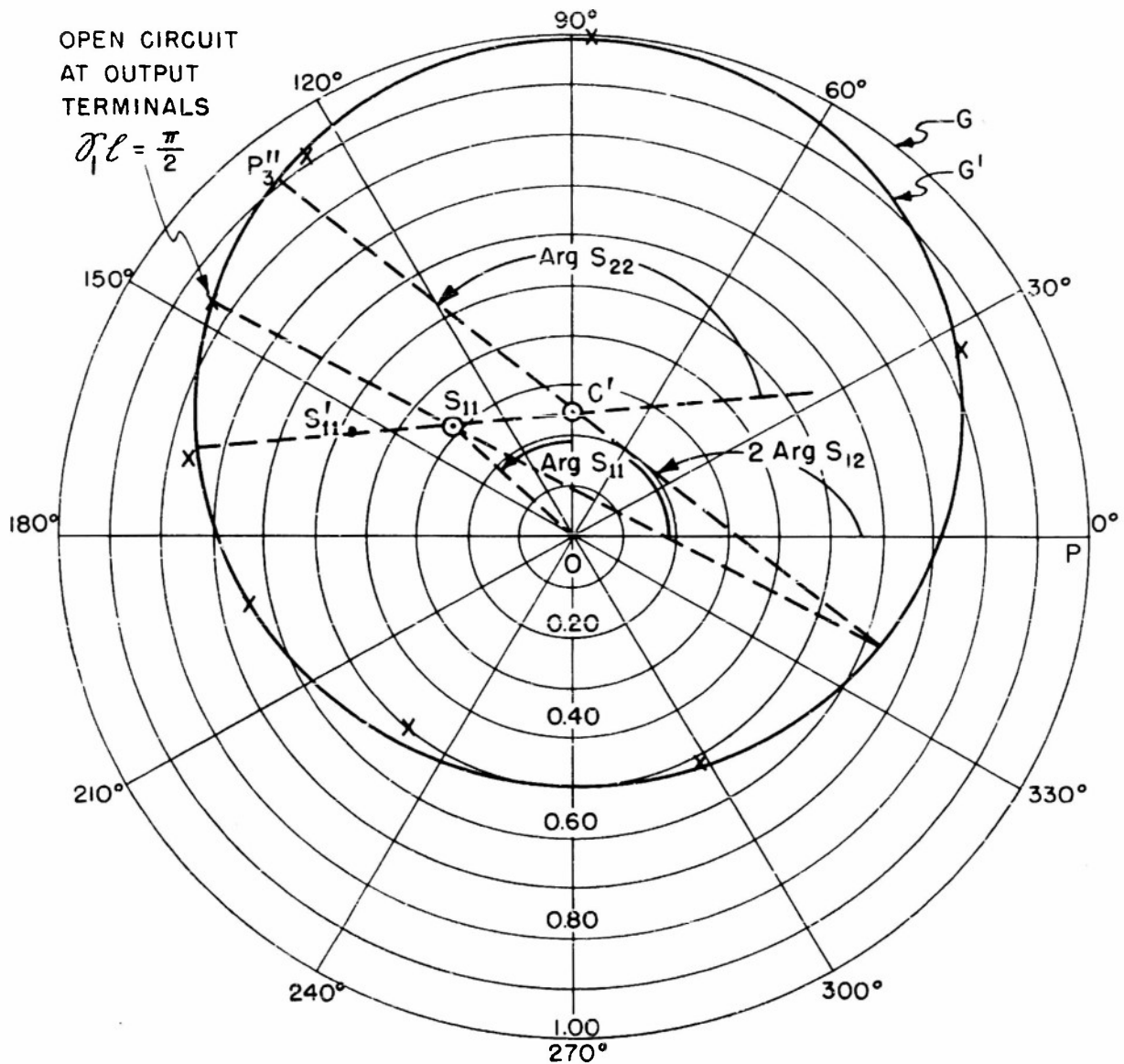


FIG. 24 GRAPHICAL DETERMINATION OF PHASE ANGLES OF SCATTERING MATRIX ELEMENTS

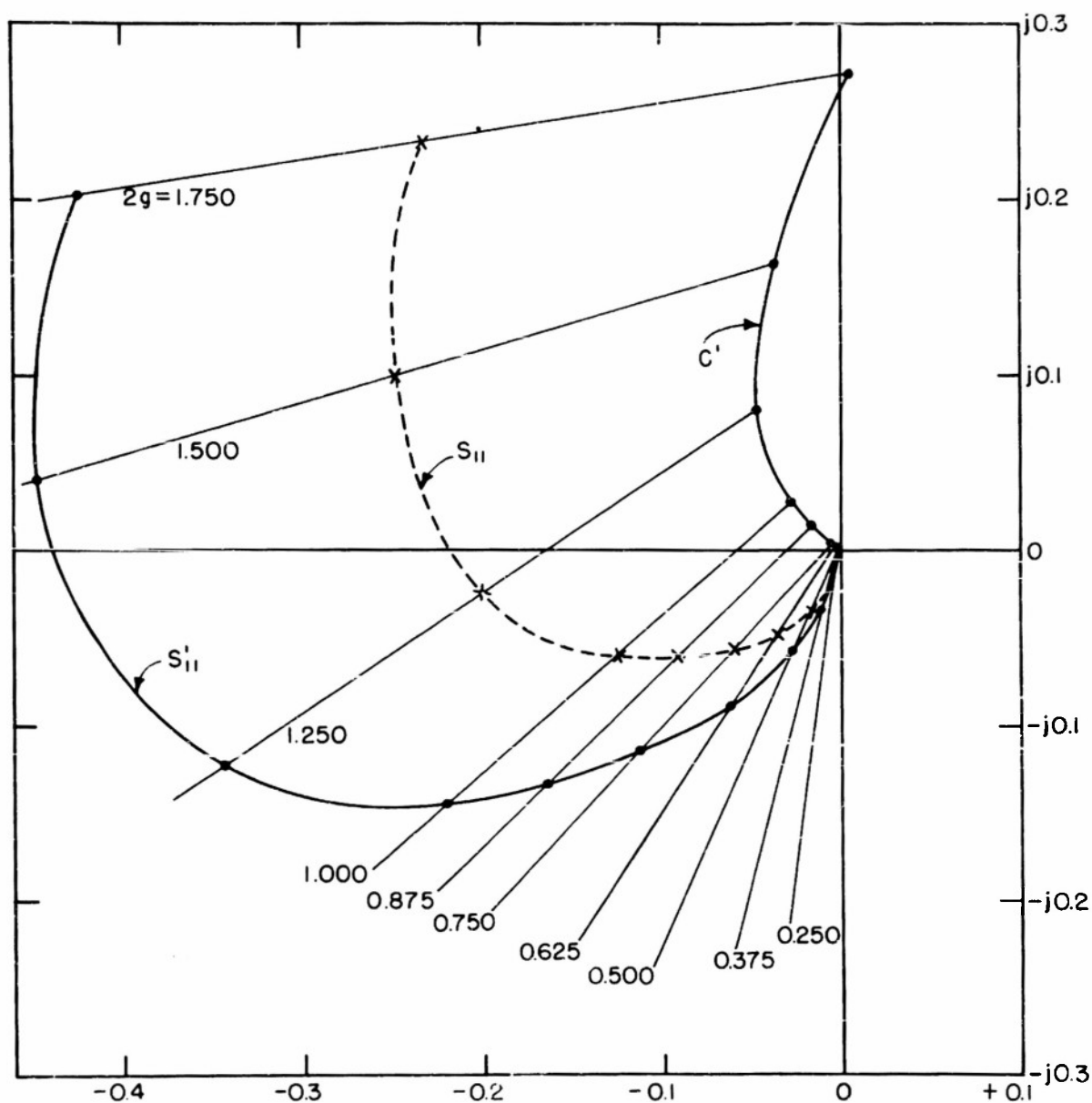


FIG. 25 LOCI OF MEASURED S'_{11} , S_{11} , AND C' ON ENLARGED REFLECTION COEFFICIENT CHART

appear as stray points. This procedure immediately indicates which particular value is in error and the experimental data can be retaken. If there is a considerable scatter of points, it is obvious that the experimental technique is incorrect or the experimental equipment faulty.

This data-refining process does not indicate if an error has been made in setting the width of the gap to a desired dimension. If this is the case, the measured elements of the scattering matrix will appear as stray points on the curves of S_{11} and S_{12} versus gap width. Again, the experimental data corresponding to the questionable value can be retaken.

Theoretical and Experimental Results

The theoretical values of the elements of the scattering matrix are obtained from the following expressions⁹

$$S_{11} = S_{22} = \frac{1}{1 + \Delta_o} - \frac{1}{1 + \Delta_e}$$

$$S_{12} = 1 - \frac{1}{1 + \Delta_o} - \frac{1}{1 + \Delta_e}$$

where

$$\Delta_e = \frac{\gamma_1^a}{\rho_1^2} \left\{ \frac{(ka)^2}{4} - j \frac{4}{\pi} \left(\frac{a}{g} \right)^2 \right\}$$

$$\Delta_o = \frac{1}{\gamma_1^a \rho_1^2} \left\{ \frac{(ka)^4}{16} - j \frac{32}{\pi} \left(\frac{a}{g} \right)^4 \right\}$$

In discussing the theoretical and experimental results, it is convenient to examine separately the absolute values and arguments of the elements of the scattering matrix. This is logical because the experimental values of amplitude and phase are determined separately by Deschamps' graphical procedure.

The absolute values of S_{11} , S_{22} , and S_{12} are given by

$$\begin{aligned} |S_{11}| &= |S_{22}| = \frac{|\Delta e - \Delta o|}{|1 + \Delta o| |1 + \Delta e|} \\ |S_{12}| &= \frac{|\Delta o \Delta e - 1|}{|1 + \Delta o| |1 + \Delta e|} \end{aligned}$$

and their arguments are found to be

$$\text{Arg } S_{11} = \text{Arg } S_{12} = \text{Arg } (\Delta e - \Delta o) - \text{Arg } (1 + \Delta o) - \text{Arg } (1 + \Delta e)$$

$$\text{Arg } S_{12} = \text{Arg } (\Delta e \Delta o - 1) - \text{Arg } (1 + \Delta o) - \text{Arg } (1 + \Delta e)$$

The experimental values are plotted on the same figure as the theoretically determined curves in Figs. 26 and 27. It is observed that the experimental values of $|S_{11}|$ and $|S_{12}|$ are in excellent agreement with the theory for values of $2g$ up to 1.000 in., corresponding to $g/\lambda = 0.127$. It should be noted that the theory is only claimed to be valid for values of $(g/\lambda)^2 \ll 1$.

As seen from the phase characteristics of S_{11} , the experimental values lie slightly above the theoretical curve for small values of $2g$. It is observed in Fig. 27 that there is again excellent agreement between experiment and theory for values of $\text{Arg } S_{12}$ such that $2g \leq 1.000$ in.

In practice one is often interested in the VSWR looking into a junction terminated in a matched load. This information is available from the results obtained by the graphical procedure. The VSWR looking into a circumferential gap terminated in a matched load can be calculated from

$$\text{VSWR} = \frac{1 + |S_{11}|}{1 - |S_{11}|}$$

Measured and calculated VSWRs are plotted in Fig. 28.

Discussion of Results

One of the obvious sources of disagreement between theoretical and experimental results is the approximate nature of the trial function used in the variational formulation. The assumed tangential electric field on the surface

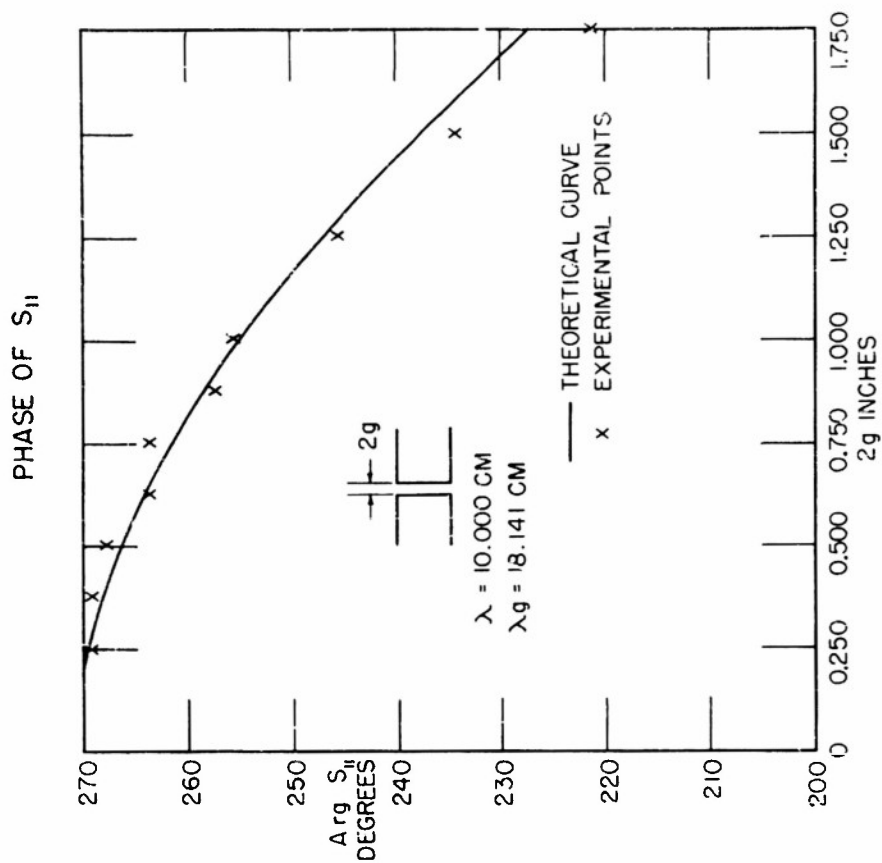
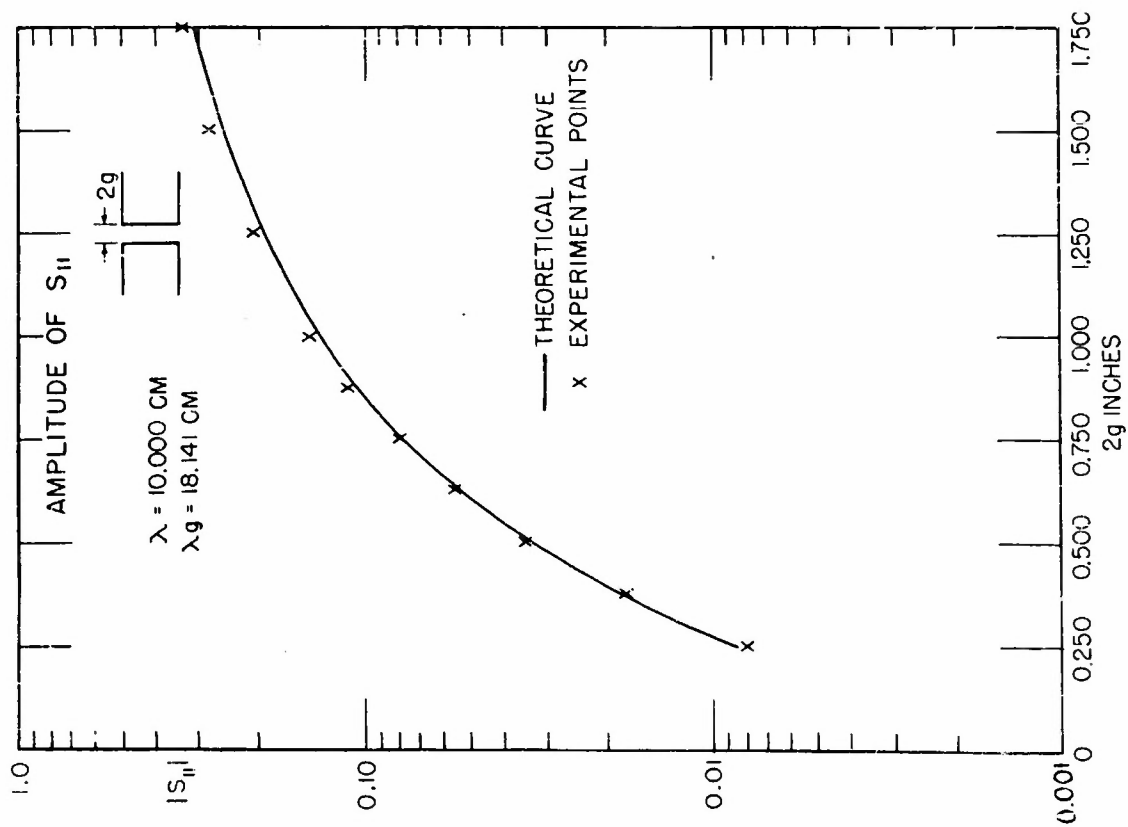


FIG. 26 MEASURED AND CALCULATED VALUES OF S_{11}

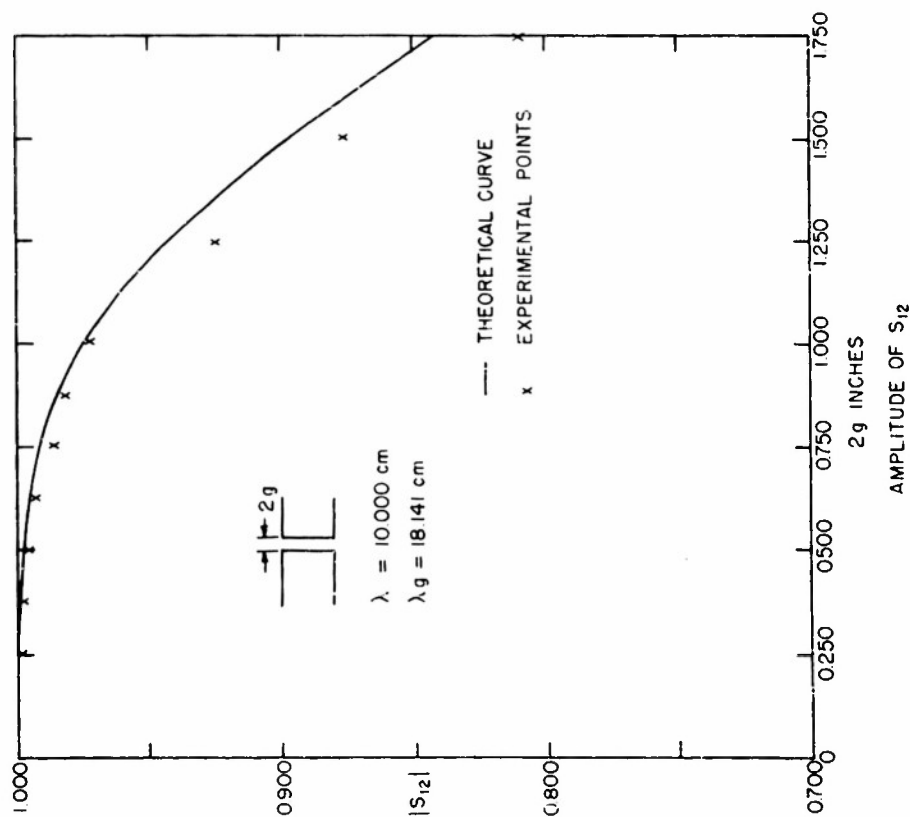
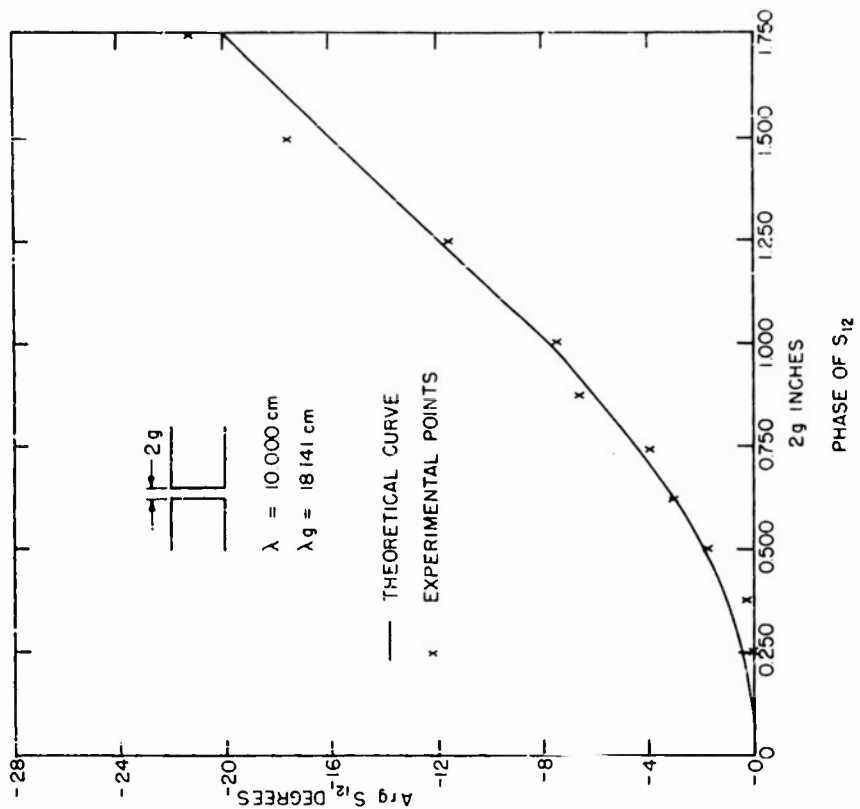


FIG. 27 MEASURED AND CALCULATED VALUES OF S_{12}

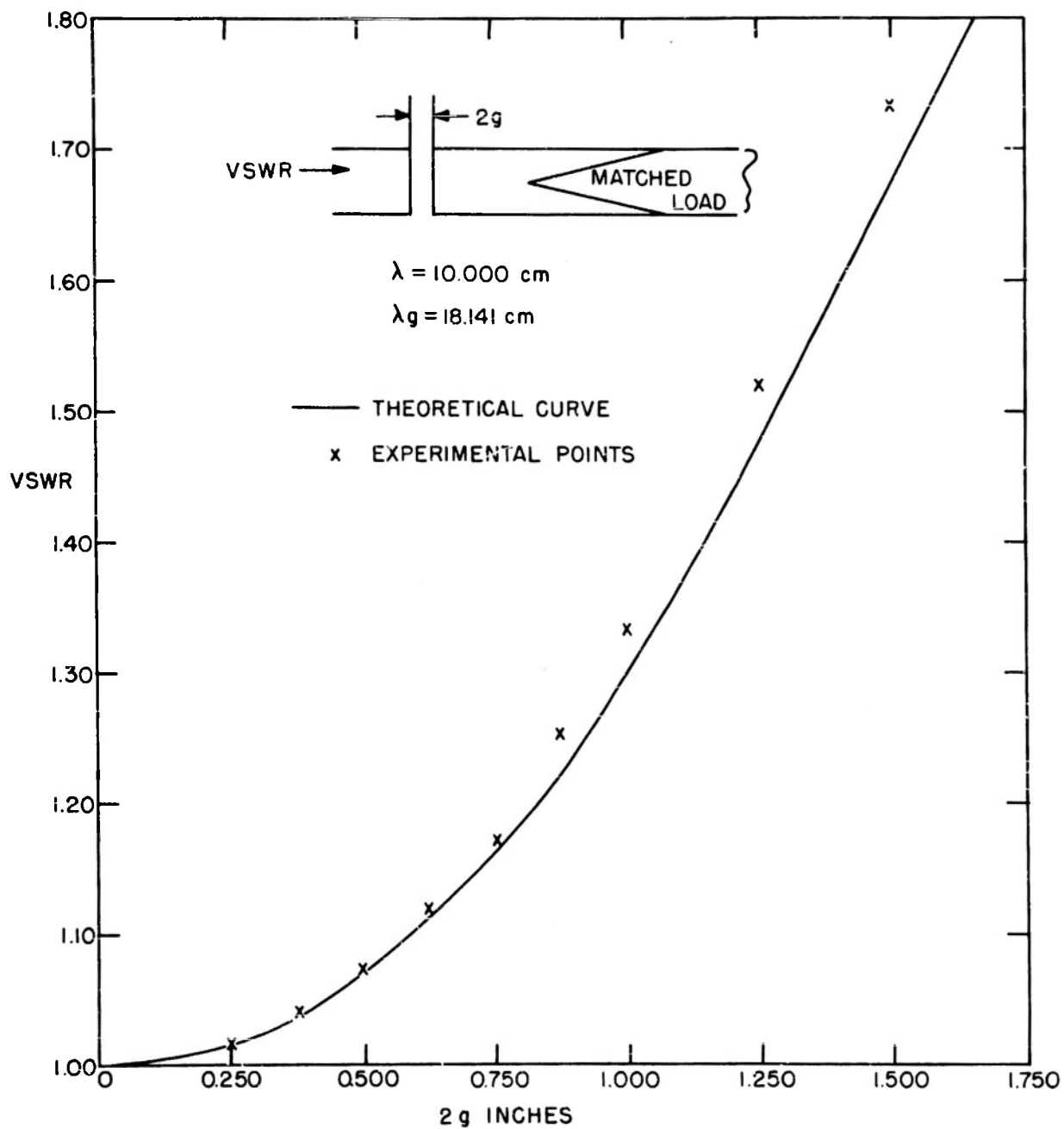


FIG. 28 VSWR OF CIRCUMFERENTIAL GAP TERMINATED IN A MATCHED LOAD

of the gap closely approximates the exact field for values of $(g/\lambda)^2 \ll 1$. In evaluating the integrals in the expressions for Δe and Δo , the "small gap" assumption is made throughout.

With regard to the experimental measurements, a reasonable check can be made by comparing the measured values of $|S_{11}|$ and $|S_{22}|$. Similarly, a comparison is made of measured values of $\text{Arg } S_{11}$ and $\text{Arg } S_{22}$. It is seen that there is excellent agreement between the measured amplitudes, whereas the differences between the measured phases tend to increase for the smaller values of $2g$. This inaccuracy in the measurement of phase can be attributed to the virtually "matched" condition that exists when the gap is so small that the graphical constructions are near the center of the reflection coefficient chart as in Fig. 25.

It appears logical to assume that the physical waveguide junction is truly symmetrical (as is borne out by examination of the physical structure as well as by the fact that the measured values of $|S_{11}|$ and $|S_{22}|$ are essentially equal); hence, the small deviations in phase are probably due to random errors in carrying out the graphical constructions.

As a partial compensation for these graphical errors, the average value of $\text{Arg } S_{11}$ and $\text{Arg } S_{22}$ is chosen as the experimental value of the phase of S_{11} (or S_{22}).^{*} It should be emphasized that this correction takes into account only what appears to be the main source of error, an error in the orientation of $\overline{S_{11}C'}$.

One concludes that the averaged measured phases of S_{11} lie slightly above the theoretical values of Fig. 26 for the smaller values of $2g$, owing to the approximate nature of the theory, random measurement errors, and small uncorrected graphical errors.

^{*}If C' practically coincides with O , one observes that an error in the measured phase of S_{11} is only an error in the orientation of $\overline{S_{11}C'}$. The error in the measured phase of S_{22} , however, is due to errors in the orientations of $\overline{S_{11}C'}$ and $\overline{C'P_3''}$. These latter deviations are caused by errors in locating respectively the pairs of points C' and P_3'' and C' and S_{11}' . Assuming that $r' \gg \overline{S_{11}C'}$ the error in the orientation of $\overline{C'P_3''}$ will then be negligible compared to the error in orientation of $\overline{S_{11}C'}$. Hence the major source of error is the same for both $\text{Arg } S_{11}$ and $\text{Arg } S_{22}$, and by inspection it is evident that this error occurs in the opposite sense for each.

The phase and magnitude of S_{12} also depend on these quantities, but the graphical determination of S_{12} is not as sensitive to the proper location of S_{11}' and C' as is the determination of the phase of S_{11} or S_{22} .

The Circumferential Gap as a Spurious Mode Suppressor

It is seen from the results of the previous sections that a small circumferential gap has a negligible effect on the transmission of the dominant circular-electric mode. This investigation leads one to inquire into the effect of the gap on other propagating modes.

To determine the gap characteristics for all propagating modes, one would be required to solve a separate boundary value problem for each propagating mode exciting the circumferential gap. For modes other than the circularly symmetrical modes, the analysis involves the solution of a vector problem instead of a scalar one. An enterprise of this magnitude is beyond the scope of this work.

It is possible, however, to draw some logical conclusions about the mode-filtering properties of the circumferential gap by evaluating the scattering matrix elements of a gap excited by the TM_{01} (dominant circular-magnetic) mode. With an approach analogous to that employed in Technical Report No. 166, one obtains the following values of Δ_e^E and Δ_o^E (the superscript E refers to the E_{01} or TM_{01} mode)

$$\Delta_e^E = \frac{2\gamma_1^E a}{\pi} \left\{ \left(\frac{\pi}{4} + \frac{\pi}{8ka} \right) - j \left(E - \ln \frac{4}{kg} \right) \right\}$$

$$\Delta_o^E = \frac{2k}{\pi \gamma_1^E} \left[\frac{\pi}{2} + \tan^{-1} \frac{J_o \left(\frac{\pi}{2} ka \right)}{Y_o \left(\frac{\pi}{2} ka \right)} \right] + j \frac{4}{\pi \gamma_1^E a} \frac{a}{g}^2$$

where

$$\gamma_1^E = \sqrt{k^2 - \left(\frac{\rho_1^E}{a} \right)^2}$$

$$J_o(\rho_1^E) = 0$$

$$\rho_1^E = 2.405$$

and

$$\bar{E} = 0.5772 \quad \text{Euler's Constant}$$

The elements of the scattering matrix are then given by

$$S_{11}^E = S_{22}^E = \frac{1}{1 + \Delta_o^E} - \frac{1}{1 + \Delta_e^E}$$

$$S_{12}^E = 1 - \frac{1}{1 + \Delta_o^E} - \frac{1}{1 + \Delta_e^E}$$

It is now convenient to introduce a mode absorbing factor M , where

$$M = 10 \log_{10} \frac{Pd^E}{Pd} \quad \text{in db}$$

in the above expression Pd^E is the power radiated by the circumferential gap when excited by a unit wave and Pd is the power radiated by the gap when excited by an incident TE_{01} wave of amplitude equal to that of the TM_{01} wave. The factor M can be expressed as a function of the scattering elements in the form

$$M = 10 \log_{10} \frac{\{1 - |S_{11}^E|^2 - |S_{12}^E|^2\}}{\{1 - |S_{11}|^2 - |S_{12}|^2\}} \quad \text{in db}$$

Theoretical curves Pd , Pd^E , and also M , as a function of gap spacing are plotted in Fig. 29. It is observed that for $2g \leq 0.250$ the power dissipated in the junction due to an incident TM_{01} wave is more than 25 db greater than that dissipated in the junction by the dominant circular-electric mode. One can conclude from the evidence of these results that a unit of several narrow gaps would serve as an effective spurious mode suppressor, while a single large gap would represent a considerable resistive loss to the desired mode as well as to the undesired modes.

Conclusion

In the preceding sections the experimental procedure used to measure the scattering matrix of a circumferential gap has been described in detail. Some attempt has been made to account for the slight differences between the experimental and theoretical results. It is concluded that these differences are caused by the approximate nature of the theory, errors in obtaining the experimental data, and the inaccuracies associated with the reduction of the experimental data by Deschamps' graphical procedure. Various experimental checks have been used to keep the possible error to a minimum value.

The next section contains a description of the measurement of the impedance of a circular waveguide excited by the dominant circular-electric mode.

IV.

MEASUREMENT OF IMPEDANCE OF RADIATING CIRCULAR WAVEGUIDE

Introduction

In this section is described the measurement of the impedance of a radiating circular waveguide. The terminal plane is chosen at the plane of the aperture and the dominant circular-electric mode is the only propagating mode in the circular tubing. The known theoretical results indicate that the open end of a circular waveguide represents an excellent match to the TE_{01} mode. Since the resonance-curve method requires $(1/VSWR)^2$ times the generator power, this method could not be used for the direct measurement of the nearly matched load over a wide band of frequencies. Consequently, a substitution method is used for the measurement of low voltage-standing-wave ratios. A comparison of experimental and theoretical results is given.

Theory

The theoretical expressions for the impedance and radiation characteristics of a semi-infinite circular guide of zero wall thickness into free space

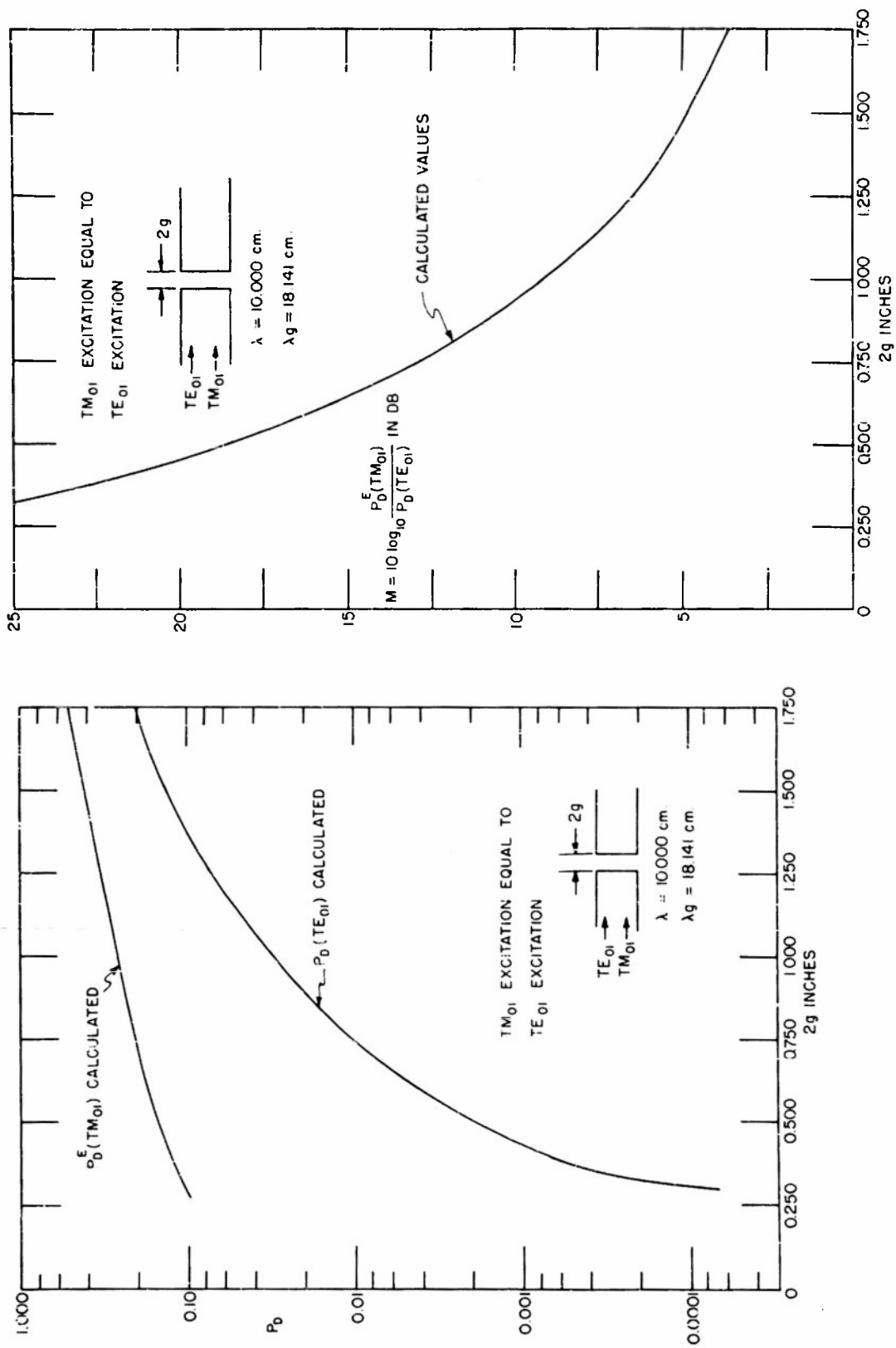


FIG. 29 MODE ABSORBING FACTOR M AS A FUNCTION OF GAP-SPACING

(TE₀₁ excitation) are presented by Marcuvitz.¹¹ The results are rigorous in the wavelength range $0.896a < \lambda < 1.64a$.

Since the theoretical results are rigorous, it is of interest to verify the theoretical values of impedance by the experimental techniques outlined in the previous sections.

Description of Experimental Arrangement

The impedance measurements were made in a closed laboratory whose dimensions are 7 feet by 12 feet. Measurements were made in a closed room to eliminate the necessity of a complicated out-of-doors set-up. Lossy cloth was applied to all nearby obstacles in order to minimize the effect of undesirable reflections. In addition, an attempt was made to maintain the circular symmetry by locating the radiating aperture as far from nearby objects as was possible in the confined space.

The measurement of impedance in an enclosed room is justified, in part, by the fact that the impedance is rather insensitive to the aperture field distribution. From the variational point of view, a first-order change in the aperture field distribution results in a second-order change in the impedance of the radiating guide.

A photograph of the open end of the circular waveguide is shown in Fig. 30. It is observed that the guide wall has an external taper which comes to a sharp edge at the plane of the radiating aperture. The purpose of the tapered edge is to approximate the boundary condition that the guide walls are infinitely thin.

The Direct Measurement of Impedance

At frequencies approaching the cutoff frequency, the impedance of the radiating guide can be measured directly. As one might expect, the voltage-standing-wave-ratio increases sharply as the operating frequency approaches that of the cutoff frequency. In the wavelength range from 11.20 to 11.98 centimeters, it is possible to make direct measurements of the desired impedance by resonance-curve method.

A Substitution Method

For $\lambda < 11.20$ cm. the impedance presented to the circular waveguide

by the radiating aperture is almost matched ($VSWR < 2$). Since the resonance-curve method is the most convenient method to measure impedances on a TE_{01} transmission line, a simple substitution method has been devised to measure low standing-wave-ratios with the existing equipment.

The equivalent transmission line is shown in Fig. 31. An obstacle of known susceptance is inserted in the transmission line at a distance d' from the plane of the aperture. The normalized admittance measured at the obstacle plane with the unknown load at the load terminals is given by

$$y_P = y_{d'} - j \frac{B}{Y_{c1}} = g_{d'} + j \left[b_{d'} - \frac{B}{Y_{c1}} \right]$$

where B/Y_{c1} is the normalized inductive susceptance of a circular obstacle, and $y_{d'}$ is the normalized input admittance of a transmission line of length d' terminated in an arbitrary load y_a .

The known susceptance is subtracted from y_P resulting in

$$y_{d'} = g_{d'} + j b_{d'}$$

The admittance of the radiating aperture is then obtained by a simple transformation of admittances along the transmission to the load. The desired impedance is just the reciprocal of this transformed admittance.

Description of Typical Impedance Measurement ... $2a/\lambda = 1.344$

The distance d' between the aperture plane and the reference plane P is determined to be 14.612 inches. This distance is determined accurately by placing a short circuit at the aperture plane and observing the resonance response. The procedure is then repeated for a short circuit located at P . The distance d' is then given by the difference in the observed resonant lengths of transmission line.

With the short circuit at P two consecutive resonances are obtained to measure the guide wavelength. For this illustrative example, the guide wavelength is measured to be 25.857 cm. The value of λ is calculated to be 10.874 cm. with $2a/\lambda = 1.344$. The short circuit is removed and thin circular obstacle of known susceptance is inserted at P . The chosen ob-

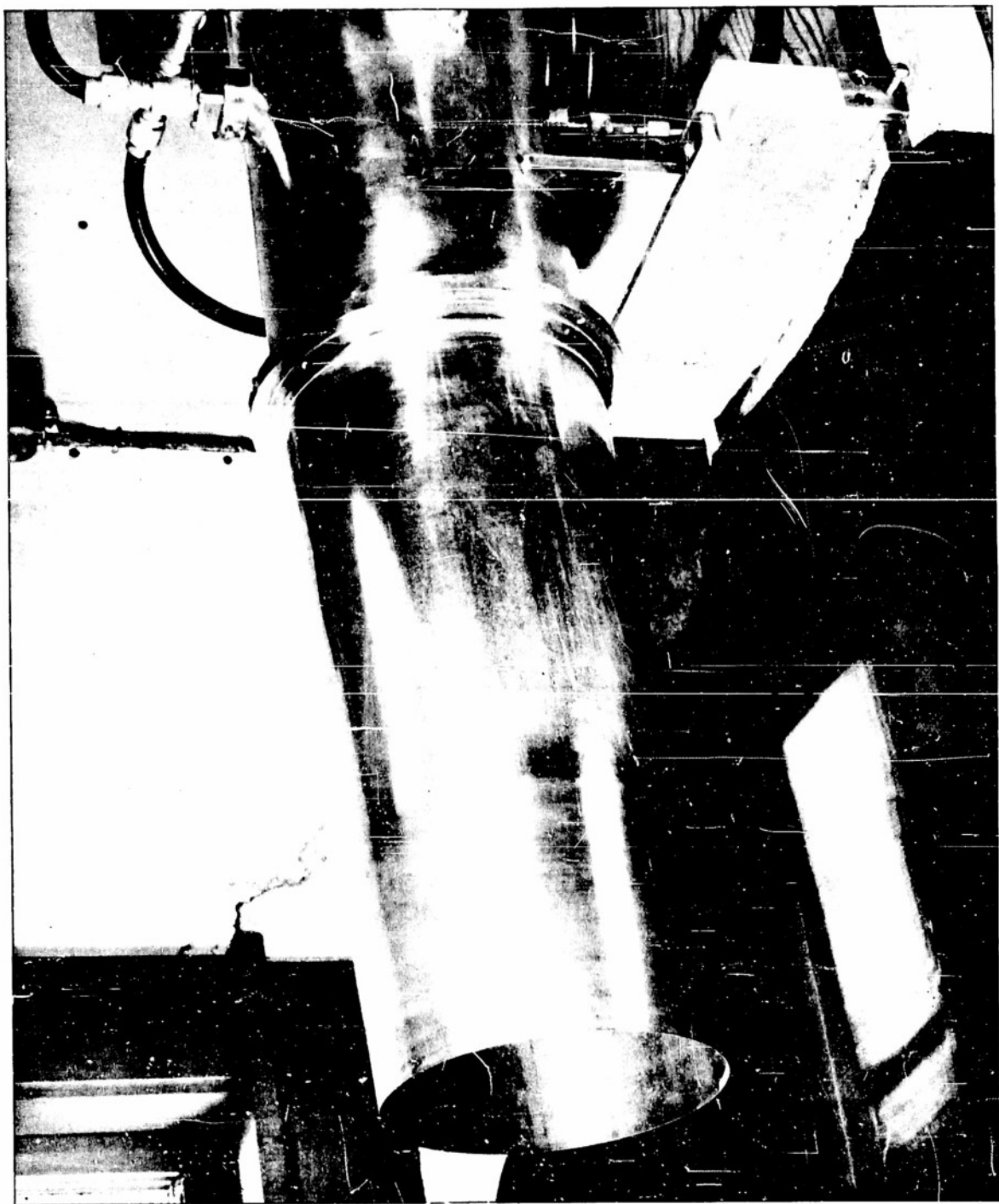


FIG. 30 OPEN END OF RADIATING CIRCULAR GUIDE

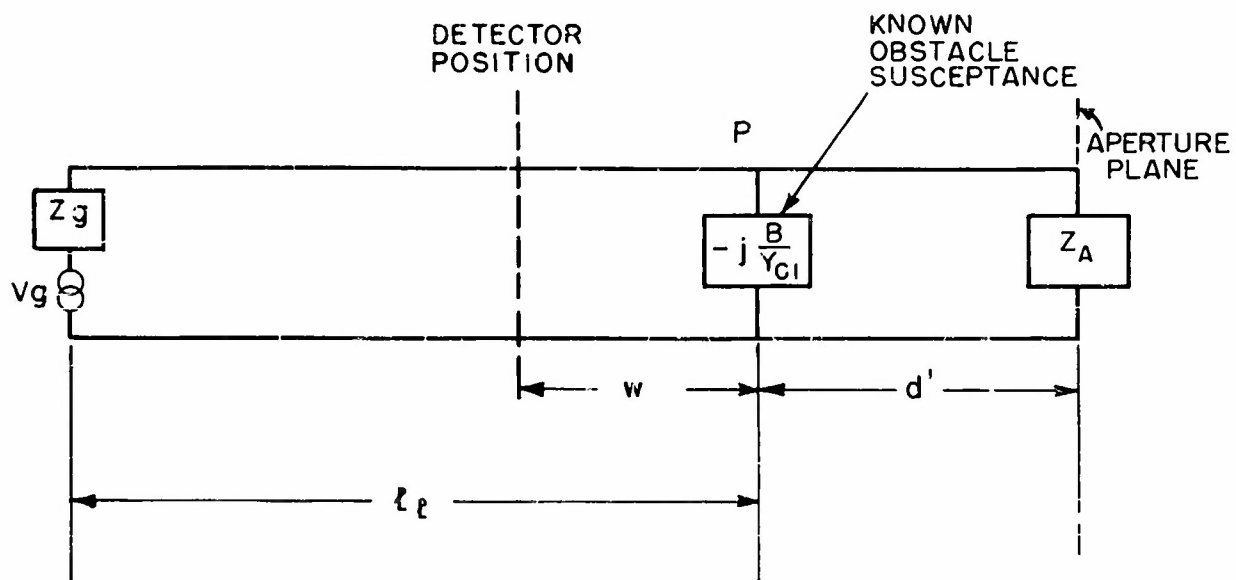


FIG. 31 EQUIVALENT TRANSMISSION-LINE CIRCUIT
USED IN THE MEASUREMENT OF IMPEDANCE
OF A RADIATING CIRCULAR GUIDE

stacle has a value of normalized susceptance of $B/Y_{cl} = 3.013$. With the obstacle in the obstacle mount and the open end of the circular waveguide radiating into space, a measurement is made of the normalized admittance y_P at P. This admittance obtained by the resonance-curve method is

$$y_P = 1.567 - j3.083$$

Subtracting the known value of inductive susceptance from y_P results in

$$y_{d'} = 1.567 - j0.070$$

To determine the admittance of the radiating aperture a transformation is made from P to the plane of the aperture. The distance from P to the open end of the guide in terms of guide wavelengths is calculated to be

$$d' = 0.4353 \lambda_g$$

Since it is desired actually to determine the normalized impedance of the radiating aperture, a quarter guide wavelength is subtracted from d'/λ_g and the transformation is made yielding

$$z_A = \frac{R_A}{Z_{cl}} + j \frac{X_A}{Z_{cl}} = 0.72 + j0.27$$

The steps in the above procedure are shown on the Smith Chart of Fig. 32.

Discussion of Results

It is observed in Fig. 33 that the measured values of R_A/Z_{cl} and X_A/Z_{cl} deviate slightly from the theoretical curves. These differences can be anticipated, for on examining the experimental data one notes that a small error in the determination of B/Y_{cl} will result in an appreciable error in the impedance of the radiating aperture. A similar situation exists when an error is made in the measurement of y_P .

In addition to these obvious sources of error, one must consider the environment in which the measurements were made. Although an enclosed room is by no means an ideal place to make measurements of the impedance of radiators, one can argue that it is not possible under any circumstances

to adjust the experimental conditions to agree with the boundary conditions imposed by the theory, i.e., a semi-infinite guide, infinitely thin walls, infinite conductivity, etc.

Furthermore, it should be stressed that the presence of unwanted propagating modes can also account for discrepancies in measurement of impedance by the resonance-curve method. However, by plotting the resonance distribution curve and examining its symmetry one can identify immediately the presence of these spurious modes.

Considering these many sources of experimental difficulties, one concludes that the agreement between theory and experiment is good. The experimental values of R_A/Z_{cl} and X_A/Z_{cl} do not deviate by more than 10 per cent from the theoretical values over the range $1.3 < 2a/\lambda < 1.6$. In this range the voltage-standing-wave-ratio measured at the aperture plane is less than 2.

Conclusion

In the preceding sections it has been shown that transmission-line techniques can be applied to the measurement of impedance in a circular waveguide supporting only the dominant circular-electric mode. The resonance-curve method has been applied to measure the characteristics of circular obstacles, circumferential gaps and radiating guides. The excellent agreement between measured and calculated values is a good indication of the accuracy of the measurements performed on the TE_{01} transmission line.

References

1. N. Marcuvitz, Waveguide Handbook, Vol. 10, M.I.T. Radiation Laboratory Series, McGraw-Hill, New York, 1951, pp. 3-7.
2. D.K. Reynolds, "Surface-Current and Charge Measurements on Flat Metal Sheets", Cruft Laboratory Technical Report No. 53, 1948, pp. 22-7.
3. Bell Laboratories Staff, Radar Systems and Components, D. Van Nostrand Co., Inc., New York, 1949, pp. 944-974.
4. C. G. Montgomery, Technique of Microwave Measurements, Vol. 11, M.I.T. Radiation Laboratory Series, McGraw-Hill, New York, 1947, pp. 322-325.

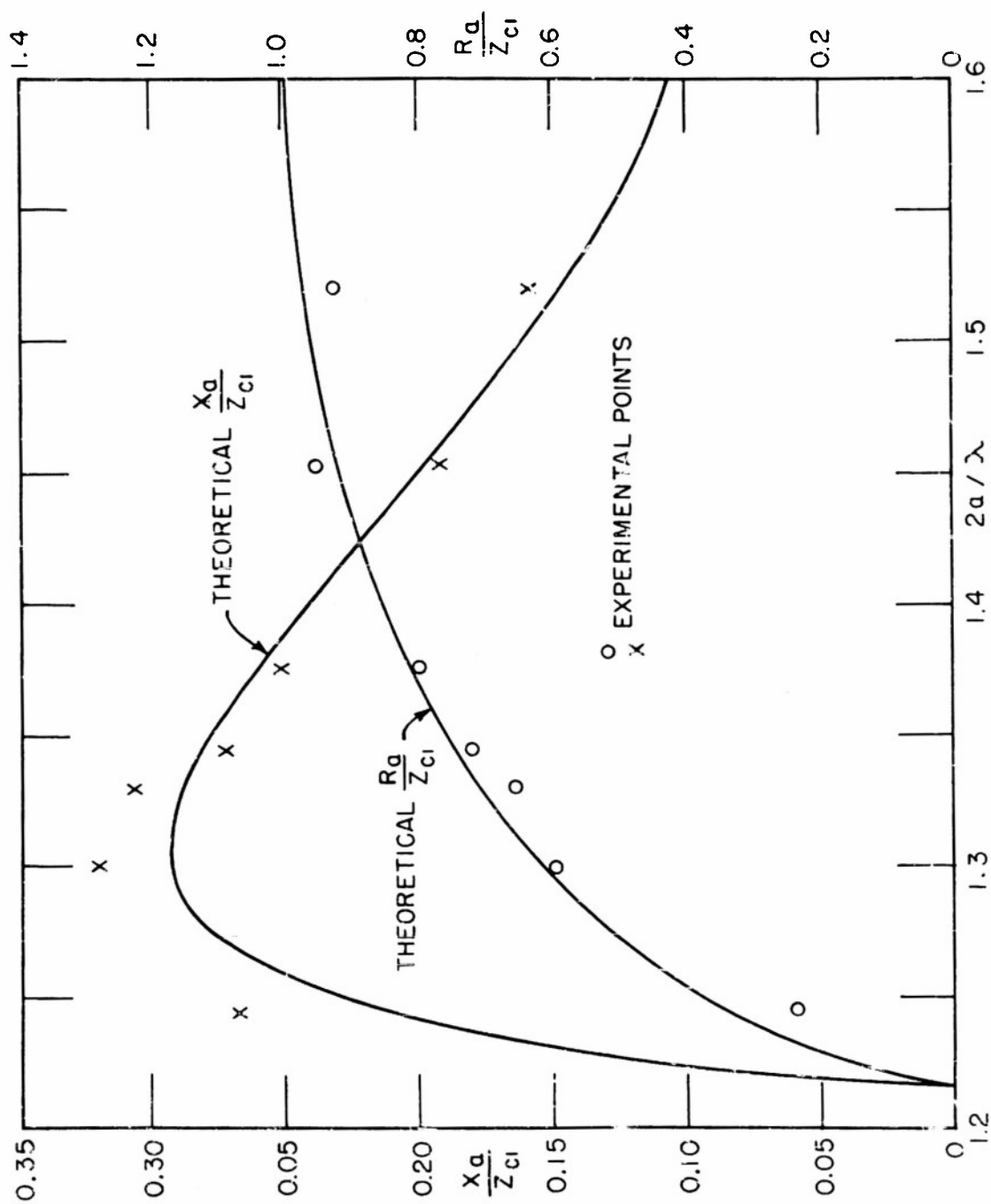


FIG. 33 THEORETICAL AND EXPERIMENTAL VALUES OF $\frac{R_a}{Z_{ci}}$ AND $\frac{X_a}{Z_{ci}}$

5. R. W. P. King, "Transmission-Line Theory and its Application", J. Appl. Phys. 14, No. 11, 577-600 (1943).
6. G. C. Southworth, Principles and Applications of Waveguide Transmission, Van Nostrand, 1950, pp. 126-129.
7. S. B. Cohn, "A Theoretical and Experimental Study of a Waveguide Structure", Cruft Laboratory Technical Report, No. 39, 1948, pp. 80-1.
8. L. S. Sheingold, "The Susceptance of a Circular Obstacle to an Incident Dominant Circular-Electric Wave", Cruft Laboratory Technical Report No. 159, 1952.
9. J. E. Storer and L. S. Sheingold, "Circumferential Gap in a Circular Waveguide Excited by a Dominant Circular-Electric Wave", Cruft Laboratory Technical Report No. 166, 1953.
10. J. E. Storer, L. S. Sheingold, S. Stein, "A Simple Graphical Analysis of Waveguide Junctions", Cruft Laboratory Technical Report No. 160, 1952.
11. N. Marcuvitz, Waveguide Handbook, Vol. 10, M.I.T. Radiation Laboratory Series, McGraw-Hill, New York, 1951, pp. 201-206.

DISTRIBUTION LIST

Technical Reports

2	Chief of Naval Research (427) Department of the Navy Washington 25, D. C.
1	Chief of Naval Research(460) Department of the Navy Washington 25, D. C.
1	Chief of Naval Research (421) Department of the Navy Washington 25, D. C.
6	Director (Code 2000) Naval Research Laboratory Washington 25, D. C.
2	Commanding Officer Office of Naval Research Branch Office 150 Causeway Street Boston, Massachusetts
1	Commanding Officer Office of Naval Research Branch Office 1000 Geary Street San Francisco 9, California
1	Commanding Officer Office of Naval Research Branch Office 1030 E. Green Street Pasadena, California
1	Commanding Officer Office of Naval Research Branch Office The John Crerar Library Building 86 East Randolph Street Chicago 1, Illinois
1	Commanding Officer Office of Naval Research Branch Office 346 Broadway New York 13, New York
3	Officer-in-Charge Office of Naval Research Navy No. 100 Fleet Post Office New York, N. Y.

1 Chief, Bureau of Ordnance (Re4)
Navy Department
Washington 25, D. C.

1 Chief, Bureau of Ordnance (AD-3)
Navy Department
Washington 25, D. C.

1 Chief, Bureau of Aeronautics (EL-1)
Navy Department
Washington 25, D. C.

2 Chief, Bureau of Ships (810)
Navy Department
Washington 25, D. C.

1 Chief of Naval Operations (Op-413)
Navy Department
Washington 25, D. C.

1 Chief of Naval Operations (Op-20)
Navy Department
Washington 25, D. C.

1 Chief of Naval Operations (Op-32)
Navy Department
Washington 25, D. C.

1 Director
Naval Ordnance Laboratory
White Oak, Maryland

2 Commander
U. S. Naval Electronics Laboratory
San Diego, California

1 Commander (AAEL)
Naval Air Development Center
Johnsville, Pennsylvania

1 Librarian
U. S. Naval Post Graduate School
Monterey, California

50 Director
Signal Corps Engineering Laboratories
Evans Signal Laboratory
Supply Receiving Section
Building No. 42
Belmar, New Jersey

3 Commanding General (RDRRP)
Air Research and Development Command
Post Office Box 1395
Baltimore 3, Maryland

2 Commanding General (RDDDE)
Air Research and Development Command
Post Office Box 1395
Baltimore 3, Maryland

1 Commanding General (WCRR)
Wright Air Development Center
Wright-Patterson Air Force Base, Ohio

1 Commanding General (WCRRH)
Wright Air Development Center
Wright-Patterson Air Force Base, Ohio

1 Commanding General (WCRE)
Wright Air Development Center
Wright-Patterson Air Force Base, Ohio

2 Commanding General (WCRET)
Wright Air Development Center
Wright-Patterson Air Force Base, Ohio

1 Commanding General (WCREO)
Wright Air Development Center
Wright-Patterson Air Force Base, Ohio

2 Commanding General (WCLR)
Wright Air Development Center
Wright-Patterson Air Force Base, Ohio

1 Commanding General (WCLRR)
Wright Air Development Center
Wright-Patterson Air Force Base, Ohio

2 Technical Library
Commanding General
Wright Air Development Center
Wright-Patterson Air Force Base, Ohio

1 Commanding General (RCREC-4C)
Rome Air Development Center
Griffiss Air Force Base
Rome, New York

1 Commanding General (RCR)
Rome Air Development Center
Griffiss Air Force Base
Rome, New York

- 2 Commanding General (RCRW)
 Rome Air Development Center
 Griffiss Air Force Base
 Rome, New York
- 6 Commanding General (CRR)
 Air Force Cambridge Research Center
 230 Albany Street
 Cambridge 39, Massachusetts
- 1 Commanding General
 Technical Library
 Air Force Cambridge Research Center
 230 Albany Street
 Cambridge 39, Massachusetts
- 2 Director
 Air University Library
 Maxwell Air Force Base, Alabama
- 1 Commander
 Patrick Air Force Base
 Cocoa, Florida
- 2 Chief, Western Division
 Air Research and Development Command
 P. O. Box 2035
 Pasadena, California
- 1 Chief, European Office
 Air Research and Development Command
 Shell Building
 60 Rue Ravenstein
 Brussels, Belgium
- 1 U. S. Coast Guard (EEE)
 1300 E Street, N. W.
 Washington, D. C.
- 1 Assistant Secretary of Defense
 (Research and Development)
 Research and Development Board
 Department of Defense
 Washington 25, D. C.
- 5 Armed Services Technical Information Agency
 Document Service Center
 Knott Building
 Dayton 2, Ohio

- 7
- 1 Director
 Division 14, Librarian
 National Bureau of Standards
 Connecticut Avenue and Van Ness St., N. W.
- 1 Director
 Division 14, Librarian
 National Bureau of Standards
 Connecticut Avenue and Van Ness St., N. W.
- 1 Office of Technical Services
 Department of Commerce
 Washington 25, D. C.
- 1 Commanding Officer and Director
 U. S. Underwater Sound Laboratory
 New London, Connecticut
- 1 Federal Telecommunications Laboratories, Inc.
 Technical Library
 500 Washington Avenue
 Nutley, New Jersey
- 1 Librarian
 Radio Corporation of America
 RCA Laboratories
 Princeton, New Jersey
- 1 Sperry Gyroscope Company
 Engineering Librarian
 Great Neck, L. I., New York
- 1 Watson Laboratories
 Library
 Red Bank, New Jersey
- 1 Professor E. Weber
 Polytechnic Institute of Brooklyn
 99 Livingston Street
 Brooklyn 2, New York
- 1 University of California
 Department of Electrical Engineering
 Berkeley, California
- 1 Dr. E. T. Booth
 Hudson Laboratories
 145 Palisade Street
 Dobbs Ferry, New York
- 1 Cornell University
 Department of Electrical Engineering
 Ithaca, New York

- 1 University of Illinois
Department of Electrical Engineering
Urbana, Illinois
- 1 Johns Hopkins University
Applied Physics Laboratory
Silver Spring, Maryland
- 1 Professor A. von Hippel
Massachusetts Institute of Technology
Research Laboratory for Insulation Research
Cambridge, Massachusetts
- 1 Director
Lincoln Laboratory
Massachusetts Institute of Technology
Cambridge 39, Massachusetts
- 1 Signal Corps Liaison Office
Massachusetts Institute of Technology
Cambridge 39, Massachusetts
- 1 Mr. Hewitt
Massachusetts Institute of Technology
Document Room
Research Laboratory of Electronics
Cambridge, Massachusetts
- 1 Stanford University
Electronics Research Laboratory
Stanford, California
- 1 Professor A. W. Straiton
University of Texas
Department of Electrical Engineering
Austin 12, Texas
- 1 Yale University
Department of Electrical Engineering
New Haven, Connecticut
- 1 Mr. James F. Trosch, Administrative Aide
Columbia Radiation Laboratory
Columbia University
538 West 120th Street
New York 27, N. Y.
- 1 Dr. J. V. N. Granger
Stanford Research Institute
Stanford, California